Plant profit maximisation improves predictions of European forest responses to drought

Article

Accepted Version

MS MANON ELISA BLEUNIENN SABOT (Orcid ID : 0000-0002-9440-4553)

DR MARTIN GERARD DE KAUWE (Orcid ID : 0000-0002-3399-9098)

Article type : Regular Manuscript

Plant profit maximisation improves predictions of European forest responses to drought

Manon E. B. Sabot[1], Martin G. De Kauwe[1], Andy J. Pitman[1], Belinda E. Medlyn[2], Anne Verhoef[3], Anna M. Ukkola[4], and Gab Abramowitz[1]

[1]ARC Centre of Excellence for Climate Extremes and Climate Change Research Centre, University of New South Wales, Sydney, NSW 2052, Australia

[2] Hawkesbury Institute for the Environment, Western Sydney University, Locked Bag 1797, Penrith, NSW 2751, Australia

[3] Department of Geography and Environmental Science, The University of Reading, PO Box 227, Reading, RG6 6AB, United Kingdom

[4] ARC Centre of Excellence for Climate Extremes and Research School of Earth Sciences, Australian National University, Canberra, ACT 0200, Australia

Corresponding Author:

This article has been accepted for publication and undergone full peer review but has not been through the copyediting, typesetting, pagination and proofreading process, which may lead to differences between this version and the Version of Record. Please cite this article as doi: 10.1111/nph.16376

Manon Sabot

Tel.: +61 293 859 766

Email: m.e.b.sabot@gmail.com

Received: *20 August 2019*

Accepted: *3 December 2019*

ORCID IDs:

Manon Sabot: 0000-0002-9440-4553

Martin De Kauwe: 0000-0002-3399-9098

Andy Pitman: 0000-0003-0604-3274

Belinda Medlyn: 0000-0001-5728-9827

Anne Verhoef: 0000-0002-9498-6696

Anna Ukkola: 0000-0003-1207-3146

Gab Abramowitz: 0000-0002-4205-001X

Summary

- Knowledge of how water stress impacts the carbon and water cycles is a key uncertainty in terrestrial biosphere models.
- We tested a new profit maximisation model, where photosynthetic uptake of CO_2 is optimally traded against plant hydraulic function, as an alternative to the empirical functions commonly used in models to regulate gas exchange during periods of water stress. We conducted a multi-

site evaluation of this model at the ecosystem scale, before and during major droughts in Europe. Additionally, we asked whether the maximum hydraulic conductance in the soil-plant continuum (k_{max}) – a key model parameter which is not commonly measured – could be predicted from long-term site climate.

- Compared to a control model with an empirical soil moisture function, the profit maximisation model improved the simulation of evapotranspiration during the growing season, reducing the Normalised Mean Square Error by *c.* 63%, across mesic and xeric sites. We also showed that k_{max} could be estimated from long-term climate, with improvements in the simulation of evapotranspiration at eight out of the 10 forest sites during drought.
- Although the generalisation of this approach is contingent upon determining k_{max}, it presents a mechanistic trait-based alternative to regulate canopy gas exchange in global models.

Key words: vegetation drought responses, land surface models, canopy gas exchange, plant optimality, plant profit maximisation, plant trait coordination, hydraulic trait adjustments to climate.

I. Introduction

Water availability is one of the primary controls of vegetation function, largely responsible for the pronounced seasonal and interannual variability in global CO_2 uptake by terrestrial ecosystems (Ahlstrom *et al.*, 2015; Jung *et al.*, 2017; Humphrey *et al.*, 2018; Green *et al.*, 2019). As a result, contemporary droughts affecting the Amazon, Australia, Europe and North America have had considerable impact on ecosystems (e.g. affecting water use efficiency, see Peters *et al.* (2018)), human populations and economic systems (Ciais *et al.*, 2005; Marengo *et al.*, 2013; van Dijk *et al.*, 2013; Boyer *et al.*, 2013). Critically, the impact of drought is often long-lasting (Kannenberg *et al.*, 2019). For example, the legacy of the 2003 European drought was apparent beyond the conclusion of the drought, as forests experienced diebacks and pest infestations (Bréda *et al.*, 2006; Stahl *et al.*, 2016). Increases in drought intensity and/or duration, as projected in response to climate change, would therefore have major implications for the terrestrial biosphere (Stocker *et al.*, 2014; Ault *et al.*, 2014; Cook *et al.*, 2015; Zhao & Dai, 2017).

In coupled climate models, land surface models (LSMs) simulate the exchange of carbon, water and energy fluxes between the land surface and the atmosphere (Pitman, 2003). Land schemes typically use empirical relationships, hereafter referred to as β functions, to reduce canopy gas exchange in response to a decline in soil water availability (Best *et al.*, 2011; Egea *et al.*, 2011). These β functions rely on soil-dependent parameters, e.g. soil moisture content at field capacity and the wilting point, instead of reflecting vegetation adaptations to water availability. β has also been defined based on soil water potential thresholds (Oleson *et al.*, 2013), causing abrupt declines in vegetation function due to declining water availability in the top soil layers (De Kauwe *et al.*, 2015b; Medlyn *et al.*, 2016). Overall, β functions lack both empirical support (Verhoef & Egea, 2014; Medlyn *et al.*, 2016) and theoretical foundation, leading to important inter-model disagreement in the shapes of the functional forms used to limit gas exchange (Desborough, 1997; Medlyn *et al.*, 2016; De Kauwe *et al.*, 2017).

Importantly, the use of β functions contradicts widespread evidence that plants differ in their sensitivity to reduced water availability (Brodribb & Cochard, 2009; Urli *et al.*, 2013; Li *et al.*, 2017). Explicit representations of plant hydraulics (segmented into e.g. root, stem, and leaf hydraulic elements) offer a mechanistic alternative to empirical soil-dependent β functions, and can be parameterised from measured plant traits (e.g. Sperry *et al.*, 1998; Williams *et al.*, 2001; Sperry & Love, 2015; Xu *et al.*, 2016; Tuzet *et al.*, 2017; Martin-StPaul *et al.*, 2017). By depicting water transport through the soil-plant-atmosphere continuum, plant hydraulic schemes open pathways to capture key vegetation responses to drought: as water availability declines, xylem water potential drops and critical cavitation might occur (Wolfe *et al.*, 2016; Martin-StPaul *et al.*, 2017), a process which could lead to representing mortality via hydraulic failure.

Another approach extends the long-standing Water Use Efficiency Hypothesis (WUEH; Cowan & Farquhar (1977); Medlyn *et al.*, (2011)) in relation to plant hydraulics (Wolf *et al.*, 2016; Sperry *et al.*, 2017). The WUEH postulates that stomata adjust to keep the relationship between the sensitivities of the stomatal conductance (g_s) to transpiration (E) and to net carbon assimilation (A_n) constant for a fixed amount of water loss (λ). Whilst the WUEH is supported by empirical data (Lin *et al.*, 2015), there is no clear way to estimate changes in λ on the timescale over which soil water changes (Wong *et al.*, 1985; Manzoni *et al.*, 2011). Consequently, the WUEH fails to relate the sensitivities of E and

A_n with a hydraulic cost of water loss and still relies on a β function to limit gas exchange (De Kauwe *et al.*, 2015a).

By contrast, Wolf *et al.* (2016) and Sperry *et al.* (2017) hypothesised that plants optimally control water loss on an instantaneous basis, to avoid excessive reduction in xylem hydraulic conductivity from a drying soil. In their approach, vulnerability curves are modelled from several set points, which correspond to specific plant hydraulic parameters, i.e. two P_x parameters representing the water potential drop at x% xylem conductivity loss (e.g. P_{50} at 50% xylem conductivity loss). It is worth highlighting that the set points used to model the vulnerability curves arise directly from measurements. The later allows for realistic simulations of the progressive impairment of water flow through the xylem, as water potential drops from the point of maximum hydraulic conductance. Unlike the WUEH, these approaches offer a mechanism to parameterise a spectrum of water use strategies, accounting for plant vulnerability to water stress.

In practice, Wolf *et al.* (2016) reformulated the WUEH, by expressing the cost of transpiration as a marginal carbon cost due to lost hydraulic conductivity, but direct measurements and/or a specific formulation of this marginal carbon cost are lacking. Sperry *et al.* (2017) overcame this limitation by normalising the water and carbon components of the WUEH, which avoids an explicit marginal cost. Their solution has since been shown to perform well at the plant scale in garden experiments (Venturas *et al.*, 2018; Wang *et al.*, 2019), but is yet to be tested at the ecosystem scale and across ecosystems.

Applying the Wolf *et al.* (2016) and Sperry *et al.* (2017) schemes in models requires three specific hydraulic parameters. Whereas values of the two required P_x parameters are readily available from hydraulic trait databases (e.g. Choat *et al.*, 2012), estimating the maximum hydraulic conductance in the soil-plant continuum (k_{max}) is more complicated. Wolf *et al.* (2016) proposed combining the conductivity from soil to the fine-root xylem, the hydraulic conductivity in the root zone, and the ratio of root to leaf area to calculate k_{max}. Venturas *et al.* (2018) and Wang *et al.* (2019) set the rhizosphere maximum hydraulic conductance and inferred the whole plant (roots to leaves) component of k_{max} from measured ratios of transpiration to leaf water potential in well-watered conditions. Either

formulation is challenging to parameterise globally and requires additional input parameters that are not readily available.

This study has two objectives:

I. to take the Sperry *et al.* (2017) model from the plant to the ecosystem scale, testing the capacity of this new model to simulate observed (eddy covariance) water and carbon fluxes across European forests during two major droughts (2003 and 2006);

II. to test whether the unknown key model parameter, k_{max} in the soil-plant continuum, can be estimated at the stand (or ecosystem) scale, assuming coordination between the hydraulic and photosynthetic traits, as well as hydraulic long-term behavioural plasticity and adjustments to climate.

To address objective I, we implemented a modified version of the Sperry *et al.* (2017) model into a simplified LSM. This allows us to test the behaviour of this new model in a generic tractable framework, respecting the broad assumptions commonly used in LSMs without making the implementation specific to an existing LSM. Inside the tractable LSM, we compared the behaviour of the modified Sperry *et al.* (2017) model to that of the Medlyn stomatal optimisation model (Medlyn *et al.*, 2011), which is widely used in state-of-the-art LSMs (CABLE (De Kauwe *et al.*, 2015a), CLM5.0 (Kennedy *et al.*, 2019), JULESv5.4 (Oliver *et al.*, 2018)). To address objective II, we explored alternative ways to determine k_{max}, testing combinations of various climatic and behavioural adjustments, but always assuming hydraulic and photosynthetic trait coordination.

II. Materials and Methods

The Materials and Methods are organised into six sections: (1) describes the modified Sperry *et al.* (2017) model; (2) presents the approaches tested to estimate k_{max}; (3) outlines the core components of the tractable LSM; (4) describes the forcing and site data; (5) details the model experiments performed; and (6) introduces a methodology to robustly assess model performance.

A summary of the model experiments and configurations (Material and Methods 3 and 5) is available in Table 3. A more visual summary of our experimental setup (Materials and Methods 5 to 6a) is

presented in the Supporting Information Fig. S1. For the site information and parameters, cf. Tables 1 and 2 and the Supporting Information Tables S1 and S2; Tables S3-S5 contain additional model parameters.

1. Profit Maximisation Approach

The approach developed by Sperry *et al.* (2017) proposes that plants regulate leaf water potential (Ψ_{leaf}; MPa) on an instantaneous basis, by trading increasingly marginal carbon intakes against increasing hydraulic conductance losses. Thus, plants balance carbon gain (CG) and hydraulic cost (HC) at the optimal leaf water potential ($\Psi_{leaf,opt}$; MPa) where profit is maximised:

$$Profit_{max} = max(CG(\Psi) - HC(\Psi)) \qquad \in [0,1] \qquad (1)$$

Ψ (MPa) is the water potential in the soil-plant continuum (see paragraph below). CG and HC are unitless and normalised to one, which makes them comparable.

In our implementation of the model introduced in Eqn 1, Ψ varies along a continuous transpiration stream (i.e. a single hydraulic conductor): from the root zone soil water potential (Ψ_s; MPa) to Ψ_{leaf}. Ψ_{leaf} cannot drop below the critical leaf water potential indicative of maximum xylem hydraulic failure (Ψ_{crit}; MPa). Using a continuous transpiration stream reduces parameterisation by removing hydraulic segmentation, but likely results in more marked drought stress because it smooths conductance changes between the root zone and the leaves. We set Ψ_{crit} to match a near complete hydraulic conductivity loss of 95%, accounting for possible high levels of embolism resistance.

a) Hydraulic Cost

The normalised hydraulic cost function reflects the increasing potential damage from cavitation as hydraulic conductance is lost:

$$HC(\Psi) = \frac{k_{i,max} - k(\Psi)}{k_{i,max} - k_{crit}} \qquad \in [0,1] \qquad (2)$$

where $k_{i,max}$ (mmol m^{-2} s^{-1} MPa^{-1}) is the instantaneous maximum hydraulic conductance in the soil-plant continuum, after accounting for water stress (i.e. k_{max} evaluated at Ψ_s), k_{crit} (mmol m^{-2} s^{-1} MPa^{-1}) is the critically low hydraulic conductance that provokes xylem failure at Ψ_{crit}, and k (mmol m^{-2} s^{-1}

MPa^{-1}) is the hydraulic conductance for any water potential in the soil-plant continuum (see Eqn 3).

Hydraulic conductance is represented by a cumulative Weibull distribution (Neufeld *et al.*, 1992):

$$k(\Psi) = k_{max}\, e^{-\left(\frac{\Psi}{b}\right)^{c}} \qquad (3)$$

where k_{max} (mmol m^{-2} s^{-1} MPa^{-1}) is the maximum hydraulic conductance in the soil-plant continuum; b (MPa) and c (unitless) are sensitivity and shape parameters of the plant hydraulic vulnerability curve, reconstructed from two P_x parameters (e.g. P_{50} and P_{88}; cf. Eqn S8 and S9).

Here, k_{max} represents the maximum conductance of a single hydraulic conductor connecting the root zone to the leaves. In segmented representations of plant hydraulic, this parameterisation would vary between the rhizosphere, roots, stem, etc. Our approach combines all the hydraulic elements in the soil-plant continuum, hence encompassing maximum rhizosphere conductance as well as maximum whole plant hydraulic conductance.

k drops with soil water depletion, owing to xylem embolism, and recovers with soil water recharge (i.e. we assume perfect and instantaneously reversible embolism). Hence, the supply of water for transpiration from the root zone depends on plant hydraulic vulnerability and photosynthetic demand (via CG in Eqn 1), for any steady-state pressure drop between Ψ_s and Ψ_{leaf} (Sperry & Love, 2015):

$$E(\Psi_{leaf}) = \int_{\Psi_s}^{\Psi_{leaf}} k(\Psi)\, d\Psi \qquad (4)$$

where E is expressed in mmol m^{-2} s^{-1}.

b) Carbon Gain

The normalised carbon gain function represents a marginally decreasing carbon gain as leaf water potential becomes more negative:

$$CG(\Psi_{leaf}) = \frac{A(\Psi_{leaf})}{A_{max}} \quad \in [0,1] \qquad (5)$$

where A (µmol m^{-2} s^{-1}) is the photosynthetic uptake at each corresponding Ψ_{leaf} and A_{max} (µmol m^{-2} s^{-1}) is the instantaneous maximum over the range of Ψ_{leaf}.

The diffusive supply of CO_2 uses Fick's first law to represent the CO_2 flux from the ambient air (C_a) into the leaf intercellular air spaces (C_i):

$$A(\Psi_{leaf}) = g_c(\Psi_{leaf})\,(C_a - C_i(\Psi_{leaf})) \qquad (6)$$

where g_c is the CO_2 diffusive leaf conductance (mol m^{-2} s^{-1}). C_i is obtained at Ψ_{leaf} by solving a system comprising Eqn 6 and a biochemical photosynthesis model (Farquhar *et al.*, 1980) of net carbon assimilation (A_n; µmol m^{-2} s^{-1}); see Supporting Information Methods S1.

In Eqn 6, g_c varies with Ψ_{leaf}. To solve for g_c, leaf-to-air vapour pressure deficit (D_{leaf}; kPa), and leaf temperature (T_{leaf}; °C) – at a given Ψ_{leaf}, we build a system of three expressions of $E(\Psi_{leaf})$: (i) E given by the supply function (Eqn 4); (ii) E meeting the atmospheric demand for water, i.e. equating $1.57 g_c D_{leaf}$ where 1.57 converts from conductance to CO_2 to total leaf conductance to water vapour; and (iii) E given by the Penman-Monteith equation following radiative and thermodynamic constraints imposed on T_{leaf} (see Eqn S7), and thus on D_{leaf}.

Whilst the second equation of this system (atmospheric demand for E) implies a perfect coupling between the leaves and the atmosphere, stomatal feedbacks are theoretically accounted for via the plant hydraulic vulnerability in the supply equation (cf. Eqn 4).

2. Calculating the Maximum Hydraulic Conductance (k_{max})

As discussed in the Introduction, the key model parameter k_{max} is not readily available. Katul *et al.* (2003) and Sperry *et al.* (2017) suggested a non-instantaneous (but not clearly defined) timescale of optimality, on which hydraulic plant traits would coordinate with photosynthetic traits. This hypothesis would reduce parameterisation and be supported by experimental evidence at the leaf- (e.g. Brodribb & Feild, 2000) and the stand-level (e.g. Lai *et al.*, 2002).

a) k_{max} behavioural plasticity

Sperry *et al.* (2017) suggested that to maintain an optimal C_i:C_a ratio of 0.7, k_{max} should be coordinated with respect to both Eqn 1 and the maximum carboxylation rate at 25°C ($V_{cmax,25}$) (cf. fig. 3b in Sperry *et al.* (2017)). With that assumption, plants always follow the profit maximisation

approach, even at longer timescales; the possibility of long-term strategies oriented toward greater carbon accumulation, or greater water conservation, is ignored.

Here, we extend the Sperry *et al.* (2017) coordination hypothesis to add two alternative solutions for k_{max}, because we have no *a priori* knowledge of how, and whether, hydraulic and photosynthetic trait coordination varies across plant species. We test the idea that a degree of plasticity in k_{max} would feed back on $\Psi_{leaf,opt}$, and by extension on the water and carbon fluxes, so as to allow for behavioural plasticity in k_{max} at longer timescales.

All our solutions for k_{max} are calculated assuming well-watered conditions. For the first solution, $k_{max,opt}$, we calculate the value of k_{max} that yields $C_i{:}C_a = 0.7$ at $\Psi_{leaf,opt}$, following Eqn 1, as Sperry *et al.* (2017) did. $\Psi_{leaf,opt}$ corresponds to levels of embolism which vary depending on the vulnerability curve, $V_{cmax,25}$, and soil water potential. For the second solution, $k_{max,high}$, we calculate the value of k_{max} that yields $C_i{:}C_a = 0.7$ immediately before Ψ_{leaf} equals P_{12}. P_{12} is the water potential at a 12% loss in xylem conductivity, which coincides with the onset of xylem embolism (Choat *et al.*, 2018). $k_{max,high}$ is independent of Eqn 1 but makes use of Eqns 3-4 and 6 and again, $k_{max,high}$ is coordinated with $V_{cmax,25}$ so as to achieve $C_i{:}C_a = 0.7$. For the third solution, $k_{max,low}$, we calculate the value of k_{max} that yields $C_i{:}C_a = 0.7$ immediately before hydraulic cost offsets net profit. Mathematically, hydraulic cost exceeds profit when $CG(\Psi) = 2HC(\Psi)$. This third solution is the one for which the percentage loss in conductivity at Ψ_{leaf} ought to be the greatest (except in cases where the parameterised vulnerability curves indicate very negative hydraulic safety margins). Eqns 2-6 are used to determine $k_{max,low}$.

$k_{max,high}$ and $k_{max,low}$ are intended as indicators of possible alternative longer-term optimisation strategies, since coordination between them and $C_i{:}C_a = 0.7$ may not always be physiologically meaningful. $C_i{:}C_a = 0.7$ might never be observed near the onset of xylem embolism for drought avoiding species, but it is unclear what a more appropriate value would be. Note, assuming these alternative set-points is analogous to assuming different soil water availabilities upon the calculation of $k_{max,opt}$.

In all three cases, once k_{max} has been calculated, it is used as an input parameter for the profit maximisation algorithm (cf. Materials and Methods 1), which simulates actual model outputs on an instantaneous basis. Figure 1 illustrates how using values of $k_{max,high}$ and $k_{max,low}$ might alter the instantaneous profit maximisation compared to $k_{max,opt}$. In Figure 1, $k_{max,high}$ maximises profit at smaller HC and CG compared to the two other solutions, displaying a more conservative water use strategy. On the contrary, $k_{max,low}$ achieves maximum profit at higher HC and CG compared to the two other solutions, displaying a more profligate water use.

Figure 1 demonstrates an example of the relative behaviours of $k_{max,opt}$, $k_{max,high}$ and $k_{max,low}$. These relative behaviours are determined by the plant's vulnerability curve and, as such, vary from species to species.

b) k_{max} adjustments to climate

Another uncertainty pertains to the coordination of k_{max} with photosynthetic traits and climate. Figure 2 displays the theoretical response of $k_{max,opt}$ (from our first k_{max} solution) to changes in atmospheric conditions. In Figure 2a, the relationship between increasing $V_{cmax,25}$ and increasing $k_{max,opt}$ is shown. As vapour pressure deficit (D) increases, $k_{max,opt}$ further increases for a given $V_{cmax,25}$, albeit logarithmically. In Figure 2b, $V_{cmax,25}$ is fixed and $k_{max,opt}$ is constrained by T_{air}; it declines above 25°C.

Figure 2 shows that assuming $T_{air} = 25$ °C and $D = 1$ kPa, as Sperry *et al.* (2017) did, might not be appropriate for the calculation of k_{max}. As such, we test two scenarios to estimate whether the previously introduced k_{max} behavioural plasticity displays further adjustment to: (i) average climatic conditions; or (ii) to hotter and drier conditions (see Materials and Methods 4. The first scenario represents the background conditions under which plants grow. The second scenario will help us gauge the degree to which they might make hydraulic adjustments to cope with extreme growing conditions.

3. Modelling Framework

We hereafter refer to the default model, embedding the Medlyn *et al.* (2011) stomatal model, as the 'Control model', and to the profit maximisation approach (see Materials and Methods 1) as the '$\text{Profit}_{\text{max}}$ model'. Both models were implemented within the same tractable LSM and forced by half-hourly meteorological inputs (i.e. photosynthetically active radiation, air temperature, precipitation, vapour pressure deficit, atmospheric pressure, and wind speed), which makes results directly comparable. Our LSM represents many of the core processes used across LSMs, albeit simplified. Notes S1 and Figures S2-S5 of the Supporting Information show a broad agreement between the Control model and the CABLE LSM (version 2.0, revision 5320; (Kowalczyk *et al.*, 2006; Wang *et al.*, 2011)). We now summarise the key features of the tractable LSM but see the Supporting Information Methods S1-S6 for more information.

We used a two-big-leaf approximation (Wang & Leuning, 1998), differentiating the radiation absorbed by sunlit and shaded leaves to simulate canopy fluxes. Soil hydrology was represented using a water balance 'tipping bucket' model.

In the Control model, water stress impacts canopy fluxes by down-regulating the slope of the sensitivity of A_n to g_s, depending on the empirical soil-moisture stress factor β:

$$\beta = \frac{\theta - \theta_{wp}}{\theta_{fc} - \theta_{wp}} \qquad (8)$$

where θ ($\text{m}^3\ \text{m}^{-3}$) is volumetric soil moisture and θ_{wp} ($\text{m}^3\ \text{m}^{-3}$) and θ_{fc} ($\text{m}^3\ \text{m}^{-3}$) are the volumetric soil moisture contents at wilting point and field capacity, respectively.

The $\text{Profit}_{\text{max}}$ model transforms θ to Ψ_s via the Clapp and Hornberger water retention equation (Clapp & Hornberger, 1978; see Eqn S11), for use in the calculations related to the transpiration stream.

4. Forcing and site data

We tested the modelling framework at 10 European eddy-covariance sites on a latitudinal gradient (cf. Table 1) over the years preceding and during two severe droughts: the 2003 continental and 2006

regional heat wave and drought events in Europe. Attention was given to diversity in climate (cf. Table 2) and forest type (cf. Table 1), to encompass a broad range of tree functional traits (cf. Table S2). Half-hourly meteorological forcing data, as well as latent heat (LE) and Gross Primary Productivity (GPP) data used to evaluate the framework, originate from the MDS gap-filled FLUXNET2015 and LaThuile datasets (http://fluxnet.fluxdata.org) and were pre-processed using the FluxnetLSM R package (v1.0; Ukkola *et al.*, 2017). The GPP data in the FLUXNET2015 and LaThuile datasets are not actually measured, but rather estimated from measured Net Ecosystem Exchange data using a night-time partitioning approach (Reichstein *et al.*, 2005).

The model was run using site-specific prescribed phenologies (see Methods S7a) derived from the 8-day MODIS MOD15A2H Version 6 Leaf Area Index (LAI) product (Myneni *et al.*, 2015). The total effective root zone depth of the 'tipping bucket' model was set between 0.3–1.20 m across sites (cf. Table S1 for the site-specific values and Methods S8a for how they were obtained). Species-specific trait data, as well as broader Plant Functional Type (PFT), parameters used to run the LSM are provided in the Supporting Information Tables S2-S5.

5. Model spin-up and experiments

Drought events were modelled by running the Control and Profit$_{max}$ models for the calendar years of drought occurrence (2003 and 2006). The years before drought (2002 and 2005) were also modelled to act as reference conditions. The Control model was spun up to initialise the root zone soil moisture state available to both the Control and the Profit$_{max}$ at the beginning of each year. This spin-up was either forced with the flux tower's meteorological record for the previous year, when available, or with the average site climatology.

a) k_{max} calibration

Objective I (see Introduction) was addressed by calibrating k_{max} to assess whether the Profit$_{max}$ model can better explain the observed LE and GPP than the Control model (cf. Notes S2 and Fig. S6 for a calibration of the Control). To calibrate k_{max}, we first calculated $k_{max,opt}$ at $T_{air} = 25$ °C and D = 1 kPa. This reference $k_{max,opt}$ was then used to generate a sequence of possible values for k_{max}. 12

values were evenly selected between 25% – 95% of $k_{max,opt}$ and a further 12 values were evenly distributed between 105% – 250% of $k_{max,opt}$. The reference $k_{max,opt}$ itself was added to the sequence, which in total led to 25 values being used as parameter inputs to run each of the drought and non-drought years. The best calibrated k_{max} value was selected following the procedure detailed below, in Section 6a of the Materials and Methods.

b) k_{max} adjustments to climate

Objective II (see Introduction) was addressed by calculating the site-level k_{max} following the strategies in Table 3: the $k_{max,opt}$, $k_{max,high}$, and $k_{max,low}$ (introduced in Materials and Methods 2a) were each adjusted depending on long-term climate. We used coarser resolution meteorological data, from the 4.03 release of the Climate Research Unit TS dataset (CRU TS v4.03; Harris *et al.*, 2014) for the 1972-2002 period, to define two contrasting climate scenarios based on T_{air} and D:

(i) an 'Average' scenario, where CRU monthly daily mean air temperature was averaged over the growing season ($T_{air,avg}$; °C), i.e. April – November between 1972-2002. Average monthly vapour pressure deficit, D_{avg} (kPa), was calculated via Tetens' equation for saturation vapor pressure (Monteith & Unsworth, 1990), using air temperature and monthly average actual vapour pressure over the growing season;

(ii) an 'Extreme' scenario, where the 90th percentile of CRU monthly average daily maximum temperature was used to calculate $T_{air,xx}$. The associated vapour pressure deficit (D_{xx}; kPa) was calculated as above.

All the $k_{max,opt}$, $k_{max,high}$, and $k_{max,low}$ were calculated for the soil water potential at saturation, given that the plants' vulnerability curves already account for sensitivity to water stress. The site average growing season weighted sunlit-shaded LAI (cf. Table 2), but not the rooting depth, was used to scale the estimates from the leaf up to the ecosystem, assuming that a composite shaded-sunlit leaf proxy is representative of the stand's most productive state (cf. Methods S7b).

Table 2 summarises the sites' climate scenario information and the composite LAIs, whereas Table 3 provides an overview of the model experiments and configurations.

6. Model Performance Assessment

We applied the benchmarking methodology from the Protocol for the Analysis of Land Surface Models (PALS) Land Surface Model Benchmarking Evaluation Project (PLUMBER; Best *et al.*, 2015) to assess model performance. This methodology combines several statistical metrics to produce a comprehensive assessment of model skill, overcoming the shortcomings of individual metrics.

Five common statistical measures were used: Normalised Mean Square Error (NMSE), Mean Absolute Error (MAE), Standard Deviation (SD), and the 5th and 95th percentile values (p_5 and p_{95}) indicative of agreement between the simulated and observed distributions. Following PLUMBER (Best *et al.*, 2015), we calculated the absolute difference between 1 and the ratio of modelled to observed SD, and the absolute distances between the modelled and observed p_5 and p_{95}.

For each statistical metric, we assigned quantile ranks between 0 (best performance) and 1 (worst performance) to the model configurations within an experiment (cf. Materials and Methods 5a and 5b), i.e. we ranked the configurations relative to what the best performance could be following a quantile distribution. We then averaged each configuration's quantile ranks across the metrics. We therefore obtained an average quantile rank for each configuration, within each experiment. Notably, unlike averaging absolute ranks, averaging quantile ranks considers the configurations' relative performance across the statistical metrics.

a) Selection of best performing configurations within each of the experiments

To select: (i) the best calibrated configuration (objective I), and (ii) the best climate configuration (Average or Extreme scenario used to derive k_{max}; objective II), we constrained the half-hourly data between April – July in 2002 and 2003. In doing so, we limited the effects of the dry downs in selecting the configurations, i.e. we did not calibrate k_{max} on the drought months in 2003 (July – October). We opted to select the best performing configurations against the observed evapotranspiration (ET) only, given that GPP is not directly observed but, rather, estimated at eddy-

covariance sites.

Although we did not train the $Profit_{max}$ model's algorithm to match the observed data, selecting the best performing configurations based on a subset of data (ET restricted between April – July in 2002 and 2003) has consequences. We expect the ET predictions to be reasonably close to the observations between April – July in 2002 and 2003, because they are in-sample. At any other time (i.e. between July – November in 2002 and 2003; and 2005 and 2006), the $Profit_{max}$ model's ET predictions will be out-of-sample. The model's ability to match the observations will then depend on: (i) its skill, e.g. in terms of partitioning ET into transpiration and soil evaporation; (ii) changes in the vegetation properties, including potential legacy effects (in 2005 and 2006) of the 2003 drought on k_{max}. By contrast with the ET predictions, the GPP predictions are always made out-of-sample.

b) Evaluating the experiments' best performing configurations and the Control model

In Section 1 of the Results, we gauge the effects of selecting each experiment's best performing configuration (i.e. best calibration and best climate configuration) against ET only. To conduct this analysis, we first evaluated the $Profit_{max}$ model's ability to simulate both ET (partially out-of-sample) and GPP (effectively out-of-sample) over the full April – November periods. Then, again, we combined the statistical metrics into quantile ranks for each of the best configurations and the Control model, relative to the observations.

7. Code

All model and analysis code are freely available from https://github.com/ManonSabot/Profit_Maximisation_European_Forests (doi: 10.5281/zenodo.3566722)

III. Results

1. Model evaluation

Figure 3 shows each site's average quantile ranks, attained by the best model configurations and by the Control model, for GPP (panels a, c) and ET (panels b, d); panels a, b show drought years and

panels c, d show non-drought years. Lower ranks equate to better overall performance and box plots on the right of the figure summarise results across the entire period. Overall for ET, the calibration (light green, average quantile rank $\mu = 0.44$) and the best $k_{max,opt}$ among the Average and Extreme scenarios (best climate configuration summarised in dark green, $\mu = 0.55$) outperformed the Control model (purple, $\mu = 0.74$). For GPP, the performances of the best calibration ($\mu = 0.56$), of the best climate configuration ($\mu = 0.59$), and of the Control model ($\mu = 0.61$) were similar. Selecting for one model output – as we did by selecting the best configurations by evaluating their skill in reproducing ET observations alone – is likely to degrade performance of other outputs (Abramowitz *et al.*, 2019; Herger *et al.*, 2019), but in the case of the $\text{Profit}_{\text{max}}$ model, it did not lead to significant losses in overall GPP performance.

The best $\text{Profit}_{\text{max}}$ configurations from the two experiments improved on the simulated ET for each individual statistical metric of performance across all sites and years, relative to the Control model (not shown in Fig. 3). ET deviations (i.e NMSE) were reduced by *c.* 63% in the best calibration and by *c.* 54% in the best climate configuration, which reflects an increase in temporal coincidence with the observations. Accuracy increased (i.e. the MAE decreased) by *c.* 29% for the best calibration and by *c.* 23 % for the best climate configuration. The error in variability (i.e. SD metric) decreased by *c.* 41% for the best calibration and by *c.* 24% for the best climate configuration. Finally, the $\text{Profit}_{\text{max}}$ displayed increased ability in better capturing the tails of the distribution, by 14% and 13% for the p_5 metric (cf. Methods 6), and by 54% and 26% for the p_{95} metric, for the best calibration and the best climate configuration, respectively.

We expected a closer fit between the observed and calibrated $\text{Profit}_{\text{max}}$ model's ET flux in the non-drought years (2002 and 2005), because k_{max} was not calibrated on the drought periods. Yet, at three sites (Parco Ticino, Puéchabon, and Roccarespampani1) the calibrated $\text{Profit}_{\text{max}}$ model better simulated ET in the drought years than in 2002 and 2005. Relative to the Control model, improvements in the simulation of ET were larger in the drought years than in 2002 and 2005, for both the $\text{Profit}_{\text{max}}$ model's best calibration and its best climate configuration. In the drought years, the $\text{Profit}_{\text{max}}$ model outperformed the Control model for ET at eight out of 10 sites. In the non-drought years, it did so at seven sites for the best calibration and at six sites for the best climate configuration

(cf. Fig. 3). Figures 4 and 5 show timeseries comparisons of the Control model with the $Profit_{max}$ model's best calibration between April – November during the drought years (the best climate configurations are shown in Figs. 6 and 7). Large improvements in the simulated simulation ET are evident at Hyytiälä, Parco Ticino, Roccarespampani1 and El Saler. At Hesse, the $Profit_{max}$ significantly reduced ET biases (cf. Figs. 4n, 6n and S7n before June), but was still outranked by the Control (cf. Fig. 3).

2. Model behaviour

In the Control model, under well-watered conditions, photosynthetic water use efficiency (WUE) is set based on the empirical g_1 parameter and stomatal sensitivity to D (see Methods S4). In the $Profit_{max}$ model, the instantaneous WUE varies optimally depending on the potential to increase carbon gain versus the incurred risk of hydraulic function loss, even under well-watered conditions. Figure 8a shows the effective g_1 parameter implied by the behaviour of the $Profit_{max}$ model across the 10 sites. At Roccaresmpampani 1 and 2, the $Profit_{max}$ model suggests a more conservative water use strategy than the Control model (lower g_1) to better match the observations. Conversely, the $Profit_{max}$ model implies a more profligate water use strategy (higher g_1) at Hyytiäla. In either case, the resulting changes in E do not linearly translate to marked changes in GPP because of the non-linear relationship between g_s and A_n (e.g. Figs. 4a, b and 5e, f). Indeed, when stomata are fully open, A_n is primarily limited by the rate of ribulose-1,5-bisphosphate (RuBP) regeneration (see Methods S1) and thus relatively insensitive to variations in stomatal conductance.

Behaviour differences between the models are also explained by their contrasting sensitivities to D. The $Profit_{max}$ approach does not *a priori* set the sensitivity to D, whereas the Control model assumes g_s to be proportional to $1/\sqrt{D}$ in the absence of water stress (Medlyn *et al.*, 2011). Both panels of Figure 8 show a wide variation in the sensitivity of g_s to D across the 10 sites, varying between 0.48 and 0.84, and 0.62 on average in line with the findings of Oren *et al.* (1999).

To understand how the $Profit_{max}$'s instantaneous regulation of WUE affects plant water use during the growing season, we analysed the best calibration's partitioning of ET into transpiration and soil evaporation, compared to that of the Control model. At all sites besides Roccarespampani 1 and 2, the

ratio of transpiration to ET was increased and the ratio of soil evaporation to ET was decreased. These changes in partitioning led to delays in the overestimations of the rate and magnitude of dry-down simulated by the Control model (seen in many LSMs; Ukkola *et al.*, 2016) by up to two months (e.g. Fig. 5f, p in the $Profit_{max}$), on par with the observations. Figure 9 illustrates how the $Profit_{max}$ mechanistically shifted the plants' ability to transpire as a function of soil water availability, from where canopy gas exchanges are maximised to where plants begin to wilt. This led to greater transpiration under drier conditions (e.g. Fig. 5j) whereby, at seven out of the 10 sites (not shown), the stomata were still not fully closed past the threshold for the wilting point of -1.5 MPa commonly used in LSMs (see Fig. 9 for an example at two sites). By contrast, the soil water potential never dropped below -0.9 MPa in the Control model.

Crucially, the $Profit_{max}$ model's ability to simulate more realistic WUEs (e.g. Figs. 4b, p and 5b, p) and to transpire for longer could lead to more realistic annual ET and GPP modelled fluxes. Puéchabon excepted, the best calibration's total ET estimates between April – November were always closer (> 75% closer at five out of 10 sites) to the observations than the Control model's. For example, at Hyytiälä, the calibrated $Profit_{max}$ model simulated a total ET of 562 mm between April – November, compared to 537 mm and 253 mm in the observed data and Control model, respectively; over that period, its total simulated GPP was 1620 g C, compared to 2055 g C and 1423 g C in the observed data and Control model, respectively.

3. Predicted stand k_{max}

In this study, we explored whether each site's stand k_{max} could be derived from the multi-decadal (30-year) climate, assuming hydraulic adjustments on that timescale. Figure 10 shows the wide range of k_{max} values (0.08–2.53 mmol m^{-2} s^{-1} MPa^{-1}) obtained from the two climate scenarios (Average and Extreme). We found those values to be in good agreement with the literature (cf. Notes S3 and Table S6 for a qualitative comparison). Even though the calculations of k_{max} were performed without knowledge of site precipitation, the linear regressions (cf. dotted lines) show increases in k_{max} with increasing Mean Annual Precipitation (MAP; see Table 2), suggesting predictable variation in the hydraulic traits across sites. The regression slope was the steepest for the Extreme scenario, with k_{max}

values ranging *c.* 2.8 times those of the Average scenario. Note that the relationship between k_{max} and MAP can partially be explained by the relationship between P_{50} and MAP (Li *et al.*, 2018), but that latter relationship alone only explains c. 1/3 of the degree of predictability in k_{max} for a given MAP because species-level values of P_{50} weaken any direct link between P_{50} data and site MAP. The expected relationship between LAI and MAP (Yang *et al.*, 2018) is not a good candidate to explain more of the predictably, as the relationship between k_{max} and MAP holds irrespectively of changes in LAI.

Where the best climate predicted k_{max} broadly agreed with the calibrated k_{max}, the $\text{Profit}_{\text{max}}$ model's climate configuration also had the ability to outperform the Control model (cf. Fig. 3). The calibrated k_{max} exceeded that of the Extreme scenario at Hyytiälä and Loobos, but otherwise lay between the values of the Average and Extreme scenarios. The $k_{max,high}$ and $k_{max,low}$ were often smaller than the $k_{max,opt}$ (e.g. Hesse in Fig. 10), as we would expect from species trying to avoid the onset of xylem embolism (Köcher *et al.*, 2012), but this was not always the case (e.g. Puéchabon where the $k_{max,opt}$ was enveloped by the $k_{max,high}$ and $k_{max,low}$, indicating higher drought-tolerance). Overall, no unique climate-driven (i.e. Average or Extreme) or behaviour-driven (i.e. $k_{max,high}$, $k_{max,opt}$, or $k_{max,low}$) pattern explained the improved model performance.

IV. Discussion

Climate models are particularly challenged when it comes to projecting how drought will change in the future (Orlowsky & Seneviratne, 2013). A number of offline LSMs have been shown to dry out too quickly (Martínez-de la Torre *et al.*, 2019; Ukkola *et al.*, 2016) and coupled-climate models markedly diverge from observations (Ukkola *et al.*, 2018) due to differences in their representation of soil hydraulic processes and vegetation water stress during drought. As root-zone soil moisture availability decreases, the partitioning of net radiation at the vegetated land surface increases sensible heat relative to latent heat. Therefore, it is likely that if climate models incorrectly represent vegetation responses to drought, they also erroneously represent feedbacks to the boundary layer (Donat *et al.*, 2018). This hinders the capacity to capture any land surface amplification of climate extremes (Miralles *et al.*, 2018; Yunusa *et al.*, 2015).

As an alternative to approaches widely used in LSMs, we investigated an optimisation approach that considers an evolving trade-off between hydraulic cost and carbon gain to limit vegetation function during periods of water stress. When calibrated (via k_{max}), the Profit$_{max}$ model was able to outperform our Control model, largely improving the simulated ET at eight out of 10 sites (cf. Fig. 3). Importantly, the Profit$_{max}$ model, with its parameterised behaviour emerging from measured hydraulic traits, showed enhanced skill both outside and during drought. During drought, the k_{max} model parameter estimated from long-term site climate also led to improvements in simulated ET at nine out of 10 sites. The positive nature of this evaluation at the ecosystem scale opens the door to the incorporation of hydraulic optimisation approaches in models.

1. Can k_{max} be derived from climate?

The Profit$_{max}$ model relies on key hydraulic traits: values of water potential relating to a specific percentage loss of conductivity (e.g. P_{50}) and k_{max}. P_x traits are widely measured; it is less clear how one might reliably estimate k_{max} at the ecosystem scale. k_{max} is a conceptual representation of the maximum conductance that plants could achieve given their ability to access water under the most favourable conditions, but it has not been commonly reported/derived in existing plant hydraulic literature. Here, we sought to explore whether k_{max} varied predictively with a measure of climate (i) because there is evidence of plant trait adjustments with climate (Atkin & Tjoelker, 2003; Carins Murphy *et al.* 2012; Marchin *et al.*, 2016; Mencuccini, 2003), and (ii) because it led to a more parsimonious model with fewer parameters.

Although MAP is a broad measure of water availability which ignores ground-water effects, we found that k_{max} increased with increasing MAP (cf. Fig. 10). This finding makes physical sense because a stand of plants with low water availability would be limited in its ability to draw water from the soil and to conduct it through to the canopy, compared to a similar stand at a location with higher water availability. We also expected k_{max} to increase with vapour pressure deficit (cf. Fig. 2a), yet be inhibited at high temperatures (cf. Fig. 2b). Across our 10 sites, we found that the Extreme climate scenario consistently predicted the highest values of k_{max}, meaning that D was the primary predictor of k_{max} in the model.

Assuming co-variation between k_{max} and $V_{cmax,25}$, we estimated k_{max} for a single value of $V_{cmax,25}$. In reality, it is likely that k_{max} varies with $V_{cmax,25}$, for instance across seasons (Wilson *et al.*, 2000), depending on factors such as climate and soil properties (which likely influence rhizosphere conductance). k_{max} is also likely to be coupled to plant allocation in individual trees (e.g. root to leaf area ratio) and to LAI and/or tree density changes at the community scale. Further difficulty arises from the range of hydraulic behaviours observed across phenotypes and within species (Aranda *et al.*, 2005), with plants adjusting their function to different climatic thresholds and/or at different timescales. At intermediate levels of precipitation (between 700 – 800 mm y^{-1}), diverse hydraulic strategies existed for similar MAPs (cf. Fig. 10).

Our attempt to estimate k_{max} based on climate is a promising proof of concept. We could further explore alternative climate descriptors, or scenarios, and alternative definitions of the stand composite LAI (which we assumed to be a fixed value), to derive k_{max}. Future work may otherwise include exploring the relation between k_{max}, (optimal ecosystem) climate, and vegetation height, not unlike Liu *et al.* (2019) who showed some coordination between hydraulic traits and maximum plant height across biomes. Approaches relying on measurements of the mean diameter of xylem, which correlates with hydraulic conductivity (cf. Hagen-Poiseuille law; Limousin *et al.*, 2010), could also be explored as they have previously been tested with some success (Cruiziat *et al.*, 2002). Finally, the use of data-driven approaches, like Bayesian model emulation (Fer *et al.*, 2018), might be an avenue for the calibration of hydraulic traits, allowing optimisation schemes to be more widely used in global LSMs.

2. Improving the simulation of GPP

Marked improvements in simulated ET, using the $\text{Profit}_{\text{max}}$ model, were not consistently followed by marked improvements to the simulation of GPP. Selecting the best configurations (see Table 3 for a reminder on what consists in a configuration) based on ET alone was likely to impair the GPP simulations because changes in ET do not linearly translate into changes in GPP. Here, remarkably, the GPP simulations were not degraded. Nevertheless, the recovery of the vegetation following an episode of drought was largely instantaneous (e.g. Fig. 5n). Indeed, the $\text{Profit}_{\text{max}}$ model only considers instantaneous fluxes and does not directly incorporate mechanistic links between loss of hydraulic function and key turnover of plant tissues (e.g. leaves; see Wolfe *et al.*, (2016) and Xu *et al.*, (2016)).

Since we prescribed LAI based on multi-year climatologies, the model could not capture large observed drops in GPP for a given year. For example, at Puéchabon, where previous years' water stress and drought legacy effects have been shown to affect leaf production in the subsequent years (Rambal *et al.*, 2014), the model failed to capture the GPP drops observed after 2003 (see the Control and $Profit_{max}$ models in Figs. 5c and S8c) because it overestimated LAI in scaling from the fluxes from the leaf-level up.

3. Implementation into state-of-the-art LSMs

Given the good performance of the $Profit_{max}$ model, implementing it into state-of-the-art LSMs to improve the representation of drought-vegetation feedbacks is an attractive option. However, it should be noted that our implementation of the profit maximisation approach assumes that the cavitation can be fully recovered upon soil water recharge (as in other hydraulic schemes, e.g. Xu *et al.*, 2016). Whilst this assumption is inconsistent with the plant hydraulic literature showing that hydraulic repair is not routine in trees (Cochard & Delzon, 2013; Delzon & Cochard, 2014), it is consistent with LSMs that do broadly not account for legacy effects. Incorporating legacy effects is a research gap for the LSM community.

Optimisation models can be perceived as computationally expensive for a climate model. Recently, Eller *et al.* (2018) proposed a simpler implementation of the Sperry et al. (2017) model with the Stomatal Optimisation Model based on Xylem Hydraulics (SOX), by removing the continuous transpiration stream. SOX changed the fundamental optimisation question asked by $Profit_{max}$ from 'what is the cavitation risk plants are willing to take to maximise carbon intake?' to 'what is the maximum carbon intake plants can achieve given a set hydraulic cost?'. We do not know how the practical simplification made by SOX might affect model behaviour across ecosystems, so it is important for future work to compare both assumptions and explore their relative merits. Until such a comparison is made, we argue in favour of maintaining a full optimisation on the transpiration stream. Besides, Venturas *et al.* (2018) have shown how the $Profit_{max}$ could be used to infer plant mortality, with the advantage of moving past prescribing mortality thresholds (Mencuccini *et al.*, 2019).

In our implementation, we used computationally optimised matrices to solve the optimisation (see code), keeping the computation expense small. We also provide a framework to vary: (i) the

frequency of instantaneous profit maximisation (i.e. Eqn 1 every 30 minutes or longer), (ii) the solving window on the transpiration stream (i.e. instead of Ψ_s to Ψ_{crit}, Ψ_s to $\Psi_{leaf,opt}(t-1) \pm x\%$ with $t-1$ being the previous timestep and the assumption that $\Psi_{leaf,opt}(t)$ would not depart by more than $x\%$ from the previous one), and (iii) the resolution of the transpiration stream itself (i.e. the increment between two adjacent Ψ). Preliminary testing (not shown) did not indicate any significant benefit from increasing the resolution of the transpiration stream (i.e. iii). Issues arose when the solving window on the transpiration stream was too narrow (i.e. ii). Lastly, whilst optimising up to every third hour did not significantly impact the simulations (i.e. i), daily optimisations flattened the model's response to environmental conditions, because they under-estimated variations in leaf water potential throughout the day.

Finally, we could apply the $\text{Profit}_{\text{max}}$ across sites globally, to generate functions to reduce stomatal conductance with decreasing soil water (e.g. Fig. S9). These functions could then be embedded in LSMs in place of the β functions. While such an approach would be empirical, it would maintain a traceable link to measurable hydraulic traits at no added computation cost to LSMs. This approach will be the subject of future work, because globally connecting hydraulic traits and water limitations on ET in land surface models used in climate models would reduce existing weaknesses during periods of water stress.

Acknowledgements

MEBS, MDK, AJP, AMU, GA acknowledge support from the Australian Research Council Centre of Excellence for Climate Extremes (CE170100023). MEBS also acknowledges support from the UNSW Scientia PhD Scholarship Scheme. MDK acknowledges support from the ARC Discovery Grant (DP190101823) and the NSW Research Attraction and Acceleration Program. AV acknowledges support from the Natural Environment Research Council grants NE/N012488/1 and NE/L010488/1. This work used eddy covariance data acquired and shared by the FLUXNET community, including these networks: AmeriFlux, AfriFlux, AsiaFlux, CarboAfrica, CarboEuropeIP, CarboItaly, CarboMont, ChinaFlux, Fluxnet-Canada, GreenGrass, ICOS, KoFlux, LBA, NECC, OzFlux-TERN, TCOS-Siberia and USCCC. The ERA- Interim reanalysis data are provided by

ECMWF and processed by LSCE. The FLUXNET eddy covariance data processing and harmonisation was carried out by the European Fluxes Database Cluster, AmeriFlux Management Project and Fluxdata project of FLUXNET, with the support of CDIAC and ICOS Ecosystem Thematic Center, and the OzFlux, ChinaFlux and AsiaFlux offices. We thank Brendan Choat for providing us with additional hydraulic trait data. Finally, we would like to thank John Sperry for his thorough comments of an earlier version of this manuscript.

References

Abramowitz G, Herger N, Gutmann E, Hammerling D, Knutti R, Leduc M, Lorenz R, Pincus R, Schmidt GA. **2019**. ESD Reviews: Model dependence in multi-model climate ensembles: weighting, sub-selection and out-of-sample testing. *Earth System Dynamics* **10**: 91–105.

Ahlstrom A, Raupach MR, Schurgers G, Smith B, Arneth A, Jung M, Reichstein M, Canadell JG, Friedlingstein P, Jain AK, *et al.* 2015. The dominant role of semi-arid ecosystems in the trend and variability of the land CO_2 sink. *Science* **348**: 895–899.

Aranda I, Gil L, Pardos JA. **2005**. Seasonal changes in apparent hydraulic conductance and their implications for water use of European beech (*Fagus sylvatica* L.) and sessile oak [*Quercus petraea* (Matt.) Liebl] in South Europe. *Plant Ecology* **179**: 155–167.

Atkin OK, Tjoelker MG. **2003**. Thermal acclimation and the dynamic response of plant respiration to temperature. *Trends in Plant Science* **8**: 343–351.

Ault TR, Cole JE, Overpeck JT, Pederson GT, Meko DM. **2014**. Assessing the Risk of Persistent Drought Using Climate Model Simulations and Paleoclimate Data. *Journal of Climate* **27**: 7529–7549.

Best MJ, Abramowitz G, Johnson HR, Pitman AJ, Balsamo G, Boone A, Cuntz M, Decharme B, Dirmeyer PA, Dong J, *et al.* 2015. The Plumbing of Land Surface Models: Benchmarking Model Performance. *Journal of Hydrometeorology* **16**: 1425–1442.

Best MJ, Pryor M, Clark DB, Rooney GG, Essery R. LH, Ménard CB, Edwards JM, Hendry MA, Porson A, Gedney N, *et al.* 2011. The Joint UK Land Environment Simulator (JULES), model description – Part 1: Energy and water fluxes. *Geoscientific Model Development* **4**: 677–699.

Boyer JS, Byrne P, Cassman KG, Cooper M, Delmer D, Greene T, Gruis F, Habben J, Hausmann N, Kenny N, *et al.* 2013. The U.S. drought of 2012 in perspective: A call to action. *Global Food Security* **2**: 139–143.

Bréda N, Huc R, Granier A, Dreyer E. **2006**. Temperate forest trees and stands under severe drought: a review of ecophysiological responses, adaptation processes and long-term consequences. *Annals of Forest Science* **63**: 625–644.

Brodribb TJ, Cochard H. **2009**. Hydraulic Failure Defines the Recovery and Point of Death in Water-Stressed Conifers. *PLANT PHYSIOLOGY* **149**: 575–584.

Brodribb TJ, Feild TS. **2000**. Stem hydraulic supply is linked to leaf photosynthetic capacity: evidence from New Caledonian and Tasmanian rainforests. *Plant, Cell and Environment* **23**: 1381–1388.

Carins Murphy MR, Jordan GJ, Brodribb TJ. **2012**. Differential leaf expansion can enable hydraulic acclimation to sun and shade: Leaf expansion can enable hydraulic acclimation. *Plant, Cell & Environment* **35**: 1407–1418.

Choat B, Brodribb TJ, Brodersen CR, Duursma RA, López R, Medlyn BE. **2018**. Triggers of tree mortality under drought. *Nature* **558**: 531–539.

Choat B, Jansen S, Brodribb TJ, Cochard H, Delzon S, Bhaskar R, Bucci SJ, Feild TS, Gleason SM, Hacke UG, *et al.* 2012. Global convergence in the vulnerability of forests to drought. *Nature* **491**: 752–755.

Ciais Ph, Reichstein M, Viovy N, Granier A, Ogée J, Allard V, Aubinet M, Buchmann N, Bernhofer Chr, Carrara A, *et al.* 2005. Europe-wide reduction in primary productivity caused by the heat and drought in 2003. *Nature* **437**: 529–533.

Clapp RB, Hornberger GM. **1978**. Empirical equations for some soil hydraulic properties. *Water Resources Research* **14**: 601–604.

Cochard H, Delzon S. **2013**. Hydraulic failure and repair are not routine in trees. *Annals of Forest Science* **70**: 659–661.

Cook BI, Ault TR, Smerdon JE. **2015**. Unprecedented 21st century drought risk in the American Southwest and Central Plains. *Science Advances* **1**: e1400082–e1400082.

Cowan IR, Farquhar GD. **1977**. Stomatal function in relation to leaf metabolism and environment. *Symposia of the Society for Experimental Biology* **31**: 471–505.

Cruiziat P, Cochard H, Améglio T. **2002**. Hydraulic architecture of trees: main concepts and results. *Annals of Forest Science* **59**: 723–752.

De Kauwe MG, Kala J, Lin Y-S, Pitman AJ, Medlyn BE, Duursma RA, Abramowitz G, Wang Y-P, Miralles DG. **2015a**. A test of an optimal stomatal conductance scheme within the CABLE land surface model. *Geoscientific Model Development* **8**: 431–452.

De Kauwe MG, Medlyn BE, Walker AP, Zaehle S, Asao S, Guenet B, Harper AB, Hickler T, Jain AK, Luo Y, *et al.* 2017. Challenging terrestrial biosphere models with data from the long-term multifactor Prairie Heating and CO_2 Enrichment experiment. *Global Change Biology* **23**: 3623–3645.

De Kauwe MG, Zhou S-X, Medlyn BE, Pitman AJ, Wang Y-P, Duursma RA, Prentice IC. **2015b**. Do land surface models need to include differential plant species responses to drought? Examining model predictions across a mesic-xeric gradient in Europe. *Biogeosciences* **12**: 7503–7518.

Delzon S, Cochard H. **2014**. Recent advances in tree hydraulics highlight the ecological significance of the hydraulic safety margin. *New Phytologist* **203**: 355–358.

Desborough CE. **1997**. The Impact of Root Weighting on the Response of Transpiration to Moisture Stress in Land Surface Schemes. *Monthly Weather Review* **125**: 1920–1930.

van Dijk AIJM, Beck HE, Crosbie RS, de Jeu RAM, Liu YY, Podger GM, Timbal B, Viney NR. **2013**. The Millennium Drought in southeast Australia (2001-2009): Natural and human causes and implications for water resources, ecosystems, economy, and society: CAUSES AND IMPACTS OF AUSTRALIA'S RECORD DROUGHT. *Water Resources Research* **49**: 1040–1057.

Donat MG, Pitman AJ, Angélil O. **2018**. Understanding and Reducing Future Uncertainty in Midlatitude Daily Heat Extremes Via Land Surface Feedback Constraints. *Geophysical Research Letters* **45**: 10,627-10,636.

Egea G, Verhoef A, Vidale PL. **2011**. Towards an improved and more flexible representation of water stress in coupled photosynthesis–stomatal conductance models. *Agricultural and Forest Meteorology* **151**: 1370–1384.

Eller CB, Rowland L, Oliveira RS, Bittencourt PRL, Barros FV, da Costa ACL, Meir P, Friend AD, Mencuccini M, Sitch S, *et al.* 2018. Modelling tropical forest responses to drought and El Niño with a stomatal optimization model based on xylem hydraulics. *Philosophical Transactions of the Royal Society B: Biological Sciences* **373**: 20170315.

Farquhar GD, Caemmerer S von, Berry JA. **1980**. A biochemical model of photosynthetic CO_2 assimilation in leaves of C_3 species. *Planta* **149**: 78–90.

Fer I, Kelly R, Moorcroft PR, Richardson AD, Cowdery EM, Dietze MC. **2018**. Linking big models to big data: efficient ecosystem model calibration through Bayesian model emulation. *Biogeosciences* **15**: 5801–5830.

Granier A, Bréda N, Longdoz B, Gross P, Ngao J. **2008**. Ten years of fluxes and stand growth in a young beech forest at Hesse, North-eastern France. *Annals of Forest Science* **65**: 704–704.

Green JK, Seneviratne SI, Berg AM, Findell KL, Hagemann S, Lawrence DM, Gentine P. **2019**. Large influence of soil moisture on long-term terrestrial carbon uptake. *Nature* **565**: 476–479.

Harris I, Jones PD, Osborn TJ, Lister DH. **2014**. Updated high-resolution grids of monthly climatic observations - the CRU TS3.10 Dataset. *International Journal of Climatology* **34**: 623–642.

Herger N, Abramowitz G, Sherwood S, Knutti R, Angélil O, Sisson SA. **2019**. Ensemble optimisation, multiple constraints and overconfidence: a case study with future Australian precipitation change. *Climate Dynamics* **53**: 1581–1596.

Humphrey V, Zscheischler J, Ciais P, Gudmundsson L, Sitch S, Seneviratne SI. **2018**. Sensitivity of atmospheric CO_2 growth rate to observed changes in terrestrial water storage. *Nature* **560**: 628–631.

Jung M, Reichstein M, Schwalm CR, Huntingford C, Sitch S, Ahlström A, Arneth A, Camps-Valls G, Ciais P, Friedlingstein P, *et al.* 2017. Compensatory water effects link yearly global land CO_2 sink changes to temperature. *Nature* **541**: 516–520.

Kannenberg SA, Novick KA, Alexander MR, Maxwell JT, Moore DJP, Phillips RP, Anderegg WRL. **2019**. Linking drought legacy effects across scales: From leaves to tree rings to ecosystems. *Global Change* Biology **25**: 2978–2992.

Katul G, Leuning R, Oren R. **2003**. Relationship between plant hydraulic and biochemical properties derived from a steady-state coupled water and carbon transport model. *Plant, Cell and Environment* **26**: 339–350.

Kennedy D, Swenson S, Oleson KW, Lawrence DM, Fisher R, Lola da Costa AC, Gentine P. **2019**. Implementing Plant Hydraulics in the Community Land Model, Version 5. *Journal of Advances in Modeling Earth Systems* **11**: 485–513.

Kivimäenpää M, Sutinen S, Calatayud V, Sanz MJ. **2010**. Visible and microscopic needle alterations of mature Aleppo pine (*Pinus halepensis*) trees growing on an ozone gradient in eastern Spain. *Tree Physiology* **30**: 541–554.

Köcher P, Horna V, Beckmeyer I, Leuschner C. **2012**. Hydraulic properties and embolism in small-diameter roots of five temperate broad-leaved tree species with contrasting drought tolerance. *Annals of Forest Science* **69**: 693–703.

Kowalczyk EA, CSIRO Marine and Atmospheric Research. **2006**. *The CSIRO Atmosphere Biosphere Land Exchange (CABLE) model for use in climate models and as an offline model*. Aspendale, Vic.: CSIRO Marine and Atmospheric Research.

Lai C-T, Katul G, Butnor J, Siqueira M, Ellsworth D, Maier C, Johnsen K, Mckeand S, Oren R. **2002**. Modelling the limits on the response of net carbon exchange to fertilization in a south-eastern pine forest. *Plant, Cell and Environment* **25**: 1095–1120.

Li X, Blackman CJ, Choat B, Duursma RA, Rymer PD, Medlyn BE, Tissue DT. **2018**. Tree hydraulic traits are coordinated and strongly linked to climate-of-origin across a rainfall gradient: Hydraulic traits coordination and link to climate. *Plant, Cell & Environment* **41**: 646–660.

Li Y, Guan K, Gentine P, Konings AG, Meinzer FC, Kimball JS, Xu X, Anderegg WRL, McDowell NG, Martinez-Vilalta J, *et al.* 2017. Estimating Global Ecosystem Isohydry/Anisohydry Using Active and Passive Microwave Satellite Data. *Journal of Geophysical Research: Biogeosciences* **122**: 3306–3321.

Limousin J-M, Longepierre D, Huc R, Rambal S. **2010**. Change in hydraulic traits of Mediterranean *Quercus ilex* subjected to long-term throughfall exclusion. *Tree Physiology* **30**: 1026–1036.

Lin Y-S, Medlyn BE, Duursma RA, Prentice IC, Wang H, Baig S, Eamus D, de Dios VR, Mitchell P, Ellsworth DS, *et al.* 2015. Optimal stomatal behaviour around the world. *Nature Climate Change* **5**: 459–464.

Liu H, Gleason SM, Hao G, Hua L, He P, Goldstein G, Ye Q. **2019**. Hydraulic traits are coordinated with maximum plant height at the global scale. *Science Advances* **5**: eaav1332.

Manzoni S, Vico G, Katul G, Fay PA, Polley W, Palmroth S, Porporato A. **2011**. Optimizing stomatal conductance for maximum carbon gain under water stress: a meta-analysis across plant functional types and climates: Optimal leaf gas exchange under water stress. *Functional Ecology* **25**: 456–467.

Marchin RM, Broadhead AA, Bostic LE, Dunn RR, Hoffmann WA. **2016**. Stomatal acclimation to vapour pressure deficit doubles transpiration of small tree seedlings with warming: Stomatal acclimation increases transpiration. *Plant, Cell & Environment* **39**: 2221–2234.

Marengo JA, Borma LS, Rodriguez DA, Pinho P, Soares WR, Alves LM. **2013**. Recent Extremes of Drought and Flooding in Amazonia: Vulnerabilities and Human Adaptation. *American Journal of Climate Change* **02**: 87–96.

Martínez-de la Torre A, Blyth E, Robinson E. **2019**. Evaluation of Drydown Processes in Global Land Surface and Hydrological Models Using Flux Tower Evapotranspiration. *Water* **11**: 356.

Martin-StPaul N, Delzon S, Cochard H. **2017**. Plant resistance to drought depends on timely stomatal closure (H Maherali, Ed.). *Ecology Letters* **20**: 1437–1447.

Medlyn BE, De Kauwe MG, Zaehle S, Walker AP, Duursma RA, Luus K, Mishurov M, Pak B, Smith B, Wang Y-P, *et al.* 2016. Using models to guide field experiments: *a priori* predictions for the CO_2 response of a nutrient- and water-limited native Eucalypt woodland. *Global Change Biology* **22**: 2834–2851.

Medlyn BE, Duursma RA, Eamus D, Ellsworth DS, Prentice IC, Barton CVM, Crous KY, De Angelis P, Freeman M, Wingate L. **2011**. Reconciling the optimal and empirical approaches to modelling stomatal conductance. *Global Change Biology* **17**: 2134–2144.

Mencuccini M. **2003**. The ecological significance of long-distance water transport: short-term regulation, long-term acclimation and the hydraulic costs of stature across plant life forms. *Plant, Cell and Environment* **26**: 163–182.

Mencuccini M, Manzoni S, Christoffersen B. **2019**. Modelling water fluxes in plants: from tissues to biosphere. *New Phytologist* **222**: 1207–1222.

Miralles DG, Gentine P, Seneviratne SI, Teuling AJ. **2018**. Land-atmospheric feedbacks during droughts and heatwaves: state of the science and current challenges: Land feedbacks during droughts and heatwaves. *Annals of the New York Academy of Sciences* **1436**: 19–35.

Monteith JL, Unsworth MH. **1990**. *Principles of environmental physics*. London ; New York : New York: E. Arnold ; Distributed in the USA by Routledge, Chapman and Hall.

Moors EJ. **2012**. Water use of forests in the Netherlands. Ph.D. thesis (290 p.) in Alterra Scientific Contributions 41, Vrije Universiteit Amsterdam, the Netherlands.

Myneni RB, Knyazikhin Y, Park T. **2015**. MOD15A2H MODIS/Terra Leaf Area Index/FPAR 8-Day L4 Global 500m SIN Grid V006 [Data set]. *NASA EOSDIS Land Processes DAAC*.

Neufeld HS, Grantz DA, Meinzer FC, Goldstein G, Crisosto GM, Crisosto C. **1992**. Genotypic Variability in Vulnerability of Leaf Xylem to Cavitation in Water-Stressed and Well-Irrigated Sugarcane. *Plant Physiology* **100**: 1020–1028.

Oleson K, Lawrence D, Bonan G, Drewniak B, Huang M, Koven C, Levis S, Li F, Riley W, Subin Z, *et al.* 2013. *Technical description of version 4.5 of the Community Land Model (CLM)*. UCAR/NCAR.

Oliver RJ, Mercado LM, Sitch S, Simpson D, Medlyn BE, Lin Y-S, Folberth GA. **2018**. Large but decreasing effect of ozone on the European carbon sink. *Biogeosciences* **15**: 4245–4269.

Oren R, Sperry JS, Katul GG, Pataki DE, Ewers BE, Phillips N, Schäfer KVR. **1999**. Survey and synthesis of intra- and interspecific variation in stomatal sensitivity to vapour pressure deficit: Intra- and interspecific variation in stomatal sensitivity to vapour pressure deficit. *Plant, Cell & Environment* **22**: 1515–1526.

Orlowsky B, Seneviratne SI. **2013**. Elusive drought: uncertainty in observed trends and short- and long-term CMIP5 projections. *Hydrology and Earth System Sciences* **17**: 1765–1781.

Peters W, van der Velde IR, van Schaik E, Miller JB, Ciais P, Duarte HF, van der Laan-Luijkx IT, van der Molen MK, Scholze M, Schaefer K, *et al.* 2018. Increased water-use efficiency and reduced CO_2 uptake by plants during droughts at a continental scale. *Nature* Geoscience **11**: 744–748.

Pilegaard K, Hummelshøj P, Jensen NO, Chen Z. **2001**. Two years of continuous CO_2 eddy-flux measurements over a Danish beech forest. *Agricultural and Forest Meteorology* **107**: 29–41.

Pitman AJ. **2003**. The evolution of, and revolution in, land surface schemes designed for climate models. *International Journal of Climatology* **23**: 479–510.

Rambal S, Joffre R, Ourcival JM, Cavender-Bares J, Rocheteau A. **2004**. The growth respiration component in eddy CO_2 flux from a Quercus ilex mediterranean forest. *Global Change Biology* **10**: 1460–1469.

Rambal S, Lempereur M, Limousin JM, Martin-StPaul NK, Ourcival JM, Rodríguez-Calcerrada J. **2014**. How drought severity constrains gross primary production(GPP) and its partitioning among carbon pools in *Quercus ilex* coppice? *Biogeosciences* **11**: 6855–6869.

Reichstein M, Falge E, Baldocchi D, Papale D, Aubinet M, Berbigier P, Bernhofer C, Buchmann N, Gilmanov T, Granier A, *et al.* 2005. On the separation of net ecosystem exchange into assimilation and ecosystem respiration: review and improved algorithm. *Global Change Biology* **11**: 1424–1439.

Rey A, Pegoraro E, Tedeschi V, De Parri I, Jarvis PG, Valentini R. **2002**. Annual variation in soil respiration and its components in a coppice oak forest in Central Italy. *Global Change Biology* **8**: 851–866.

Rinne J. **2000**. Canopy scale monoterpene emissions of *Pinus sylvestris* dominated forests. *Atmospheric Environment* **34**: 1099–1107.

Rodrigues A, Pita G, Mateus J, Kurz-Besson C, Casquilho M, Cerasoli S, Gomes A, Pereira J. **2011**. Eight years of continuous carbon fluxes measurements in a Portuguese eucalypt stand under two main events: Drought and felling. *Agricultural and Forest Meteorology* **151**: 493–507.

Sabot MEB. 2019. Profit_Maximisation_European_Forests. doi: 10.5281/zenodo.3566722

Sperry JS, Adler FR, Campbell GS, Comstock JP. **1998**. Limitation of plant water use by rhizosphere and xylem conductance: results from a model. *Plant, Cell and Environment* **21**: 347–359.

Sperry JS, Love DM. **2015**. What plant hydraulics can tell us about responses to climate-change droughts. *New Phytologist* **207**: 14–27.

Sperry JS, Venturas MD, Anderegg WRL, Mencuccini M, Mackay DS, Wang Y, Love DM. **2017**. Predicting stomatal responses to the environment from the optimization of photosynthetic gain and hydraulic cost: A stomatal optimization model. *Plant, Cell & Environment* **40**: 816–830.

Stahl K, Kohn I, Blauhut V, Urquijo J, De Stefano L, Acácio V, Dias S, Stagge JH, Tallaksen LM, Kampragou E, *et al.* 2016. Impacts of European drought events: insights from an international database of text-based reports. *Natural Hazards and Earth System Sciences* **16**: 801–819.

Stocker TF, Qin D, Plattner G-K, Tignor M, Allen SK, Boschung J, Nauels A, Xia Y, Bex V, Midgley PM. **2014**. *Climate change 2013: The physical science basis*. Cambridge University Press Cambridge, UK, and New York.

Tuzet A, Granier A, Betsch P, Peiffer M, Perrier A. **2017**. Modelling hydraulic functioning of an adult beech stand under non-limiting soil water and severe drought condition. *Ecological Modelling* **348**: 56–77.

Ukkola AM, De Kauwe MG, Pitman AJ, Best MJ, Abramowitz G, Haverd V, Decker M, Haughton N. **2016**. Land surface models systematically overestimate the intensity, duration and magnitude of seasonal-scale evaporative droughts. *Environmental Research Letters* **11**: 104012.

Ukkola AM, Haughton N, De Kauwe MG, Abramowitz G, Pitman AJ. **2017**. FluxnetLSM; R package (v1.0): a community tool for processing FLUXNET data for use in land surface modelling. *Geoscientific Model Development* **10**: 3379–3390.

Ukkola AM, Pitman AJ, De Kauwe MG, Abramowitz G, Herger N, Evans JP, Decker M. **2018**. Evaluating CMIP5 Model Agreement for Multiple Drought Metrics. *Journal of Hydrometeorology* **19**: 969–988.

Urli M, Porte AJ, Cochard H, Guengant Y, Burlett R, Delzon S. **2013**. Xylem embolism threshold for catastrophic hydraulic failure in angiosperm trees. *Tree Physiology* **33**: 672–683.

Valentini R, Miglietta F (Eds.). **2015**. *The Greenhouse Gas Balance of Italy*. Berlin, Heidelberg: Springer Berlin Heidelberg.

Venturas MD, Sperry JS, Love DM, Frehner EH, Allred MG, Wang Y, Anderegg WRL. **2018**. A stomatal control model based on optimization of carbon gain versus hydraulic risk predicts aspen sapling responses to drought. *New Phytologist* **220**: 836–850.

Verhoef A, Egea G. **2014**. Modeling plant transpiration under limited soil water: Comparison of different plant and soil hydraulic parameterizations and preliminary implications for their use in land surface models. *Agricultural and Forest Meteorology* **191**: 22–32.

Wang Y-P, Kowalczyk E, Leuning R, Abramowitz G, Raupach MR, Pak B, van Gorsel E, Luhar A. **2011**. Diagnosing errors in a land surface model (CABLE) in the time and frequency domains. *Journal of Geophysical Research* **116**. doi: 10.1029/2010JG001385

Wang Y-P, Leuning R. **1998**. A two-leaf model for canopy conductance, photosynthesis and partitioning of available energy I: *Agricultural and Forest Meteorology* **91**: 89–111.

Wang Y, Sperry JS, Venturas MD, Trugman AT, Love DM, Anderegg WRL. **2019**. The stomatal response to rising CO_2 concentration and drought is predicted by a hydraulic trait-based optimization model. *Tree Physiology* **39**: 1416–1427.

Williams M, Bond BJ, Ryan MG. **2001**. Evaluating different soil and plant hydraulic constraints on tree function using a model and sap flow data from ponderosa pine. *Plant, Cell and Environment* **24**: 679–690.

Wilson KB, Baldocchi DD, Hanson PJ. **2000**. Spatial and seasonal variability of photosynthetic parameters and their relationship to leaf nitrogen in a deciduous forest. *Tree Physiology* **20**: 565–578.

Wolf A, Anderegg WRL, Pacala SW. **2016**. Optimal stomatal behavior with competition for water and risk of hydraulic impairment. *Proceedings of the National Academy of Sciences* **113**: E7222–E7230.

Wolfe BT, Sperry JS, Kursar TA. **2016**. Does leaf shedding protect stems from cavitation during seasonal droughts? A test of the hydraulic fuse hypothesis. *New Phytologist* **212**: 1007–1018.

Wong S-C, Cowan IR, Farquhar GD. **1985**. Leaf Conductance in Relation to Rate of CO_2 Assimilation: III. Influences of Water Stress and Photoinhibition. *Plant Physiology* **78**: 830–834.

Xu X, Medvigy D, Powers JS, Becknell JM, Guan K. **2016**. Diversity in plant hydraulic traits explains seasonal and inter-annual variations of vegetation dynamics in seasonally dry tropical forests. *New Phytologist* **212**: 80–95.

Yang J, Medlyn BE, De Kauwe MG, Duursma RA. **2018**. Applying the Concept of Ecohydrological Equilibrium to Predict Steady State Leaf Area Index. *Journal of Advances in Modeling Earth Systems* **10**: 1740–1758.

Yunusa IAM, Eamus D, Taylor D, Whitley R, Gwenzi W, Palmer AR, Li Z. **2015**. Partitioning of turbulent flux reveals contrasting cooling potential for woody vegetation and grassland during heat waves: Turbulent Flux Over Grassland and Woody Vegetation Covers. *Quarterly Journal of the Royal Meteorological Society* **141**: 2528–2537.

Zhao T, Dai A. **2017**. Uncertainties in historical changes and future projections of drought. Part II: model-simulated historical and future drought changes. *Climatic Change* **144**: 535–548.

Authors Contributions

MEBS, MGDK, and AJP designed the experiments. AMU pre-processed the eddy covariance data. MEBS developed the theory, implemented the model, and performed the analysis. MEBS, MGDK, AJP, BEM, AV, AMU, and GA all contributed to the final manuscript.

Tables

Table 1. Summary of the 10 eddy-covariance sites

Site name	Country	Latitude	Longitude	PFT[a]	Dominant Species	Data[b]	Reference
Hyytiälä	Finland	61.85°N	24.29°E	ENF	*Pinus sylvestris*	FN	Rinne *et al.* (2000)
Sorø	Denmark	55.49°N	11.64°E	DBF	*Fagus sylvatica*	FN	Pilegaard *et al.* (2001)
Loobos	Netherlands	52.17°N	5.74°E	ENF	*Pinus sylvestris*	FN	Moors (2012)
Hesse Forest-Sarrebourg	France	48.67°N	7.07°E	DBF	*Fagus sylvatica*	LT[c]	Granier *et al.* (2008)
Parco Ticino Forest	Italy	45.20°N	9.06°E	DBF	*Populus x canadensis*	FN[c]	Valentini & Miglietta (2015)
Puéchabon	France	43.74°N	3.60°E	EBF	*Quercus ilex*	FN	Rambal *et al.* (2004)
Roccarespampani1	Italy	42.41°N	11.93°E	DBF	*Quercus cerris*	FN	Rey *et al.* (2002)
Roccarespampani2		42.39°N	11.92°E				
El Saler1	Spain	39.35°N	0.32°W	ENF	*Pinus halepensis*	LT[c]	Kivimäenpää *et al.* (2010)
Espirra	Portugal	38.64°N	8.60°W	EBF	*Eucalyptus globulus*	LT[c]	Rodrigues *et al.* (2011)

[a] Plant functional types (PFTs) are defined as: evergreen needleleaf forest (ENF), evergreen broadleaf forest (EBF), deciduous broadleaf forest (DBF)

[b] Datasets are either FLUXNET2015 (FN) or LaThuile (LT)

[c] Data for the years 2002 and 2003 only are used, either due to a lack of availability in the later years (LT dataset), or to missing data (at Parco Ticino Forest)

Table 2. Climate information and average growing season weighted Leaf Area Index (LAI_{gs}) at the 10 eddy-covariance sites

Site name	**Köppen Climate Class**[a]	**MAP**[b] (mm y^{-1})	$T_{air,avg}$[b] (°C)	D_{avg}[b] (kPa)	$T_{air,xx}$[b] (°C)	D_{xx}[b] (kPa)	**LAI_{gs}**[c] (m^2 m^{-2})
Hyytiälä	Dfc	570	9.88	0.34	20.20	1.19	1.34
Sorø	Cfb	568	12.82	0.31	19.70	0.77	1.58
Loobos	Cfb	778	13.40	0.34	22.00	1.14	1.34
Hesse Forest-Sarrebourg	Cfb	753	14.29	0.48	23.50	1.36	2.31
Parco Ticino Forest	Cfa	1026	18.14	0.69	28.00	1.95	0.76
Puéchabon	Csa	772	17.56	0.77	28.00	2.39	1.13
Roccarespampani1	Csa	675	19.71	0.79	29.40	2.13	1.83
Roccarespampani2							1.64
El Saler1	Csa	383	21.29	0.90	30.00	2.21	0.67
Espirra	Csa	736	20.02	0.84	29.00	2.34	0.85

[a] Köppen Climate Classes are defined as: continental without dry season and with cold summer (Dfc), temperate without dry season and with warm summer (Cfb), temperate without dry season and with hot summer (Cfa), temperate with dry and hot summer (Csa)

[b] MAP (Mean Annual Precipitation), average (*avg*) and extreme (*xx*) temperature and vapour pressure deficit values are calculated using the CRU TS v4.03 datasets (Harris *et al.*, 2014) over the 1972-2002 period

[c] Average weighted sunlit-shaded LAI values are calculated over the growing season (i.e. April – November) following the procedure detailed in the Supporting Information Methods S7b.

Table 3. Summary of the two experiments conducted to estimate the maximum hydraulic conductance (k_{max}) and of the model configurations evaluated within each experiment

	Experiments			
	Calibration	**Adjustments to climate**		
Profit$_{max}$ Configurations	25 values around the $k_{max,opt}$ at $T_{air} = 25$ °C and $D = 1$ kPa	six k_{max} values: three solutions × two climate scenarios		
		$k_{max,high}$	$k_{max,opt}$	$k_{max,low}$
		Average Scenario		Extreme Scenario

Figure Captions

Fig. 1. An example of the instantaneous profit maximisation algorithm. The carbon gain (green), hydraulic cost (purple), and net profit (blue) are shown as functions of the transpiration stream, which ranges between the soil water potential at saturation (Ψ_{sat}) and the critical water potential (Ψ_{crit}). Maximum hydraulic conductance (k_{max}) was calculated for each of the three behavioural solutions (i.e. $k_{max,high}$, $k_{max,opt}$, and $k_{max,low}$; cf. Section 2 of the Materials and Methods), before being used as an input the model. The dashed and dotted lines illustrate the impacts of alternative strategies for k_{max} on the maximum profit; the optimal leaf water potentials ($\Psi_{leaf,opt}$) at which profit is maximised span a range of 0.4 MPa between the instantaneous model run using $k_{max,high}$ and the one using $k_{max,low}$. The species used in this example is *Juniperus virginiana* ($P_{50} = -6.6$ MPa and $P_{88} = -10.5$ MPa; Choat *et al.*, 2012), with $V_{cmax,25} = 100$ µmol m^{-2} s^{-1}, $T_{air} = 25$ °C and $D = 1$ kPa, $\Psi_s = -0.8$ kPa, and LAI $= 2$ m^2 m^{-2}.

Fig. 2. The sensitivity of the modelled optimal coordination between the maximum hydraulic conductance ($k_{max,opt}$) and **(a)** the maximum carboxylation rate at 25°C ($V_{cmax,25}$) and **(b)** air temperature (T_{air}), both depending on vapour pressure deficit (D). In panel a, $k_{max,opt}$ increases near proportionally with $V_{cmax,25}$ and in a logarithmic fashion with D; T_{air} is fixed to 25 °C. In panel b, $k_{max,opt}$ increases with T_{air}, before decreasing (sharply at the two highest D) starting between 20 – 25 °C; $V_{cmax,25}$ is set to 100 µmol m^{-2} s^{-1}. The valid range for $k_{max,opt}$ is constrained by physically plausible co-occurring values of T_{air} and D under a relative humidity spanning 5 – 95%. The species used in this example is *Juniperus virginiana* ($P_{50} = -6.6$ MPa and $P_{88} = -10.5$ MPa; Choat *et al.*, 2012), with $\Psi_s = -0.8$ kPa and LAI $= 2$ m^2 m^{-2}.

Fig. 3. Quantile ranks of the best configurations of the Profit$_{max}$ model compared to the Control model, across drought (panels a and b) and non-drought years (panels c and d), and for Gross Primary Productivity (GPP; panels a and c) and Evapotranspiration (ET; panels b and d). The vertical lines – blue (Average scenario) or red (Extreme scenario) – correspond to the best climate configuration range of ranks across the three behavioural solutions for the maximum hydraulic conductance. The box and whisker plots to the right of the figure show summaries of the ranks across sites, but do not

account for the behavioural range shown by the vertical lines. In the box and whiskers plots, the horizontal yellow line shows the average overall quantile rank, and the box shows the interquartile range; the whiskers extend to the 10th and 90th percentile values of the ranks, with dots outside of the whiskers showing outliers.

Fig. 4. A 14-day running average of the carbon and water fluxes predicted by the best selected calibration configuration from the Profit$_{max}$ model (green line) at the five northernmost eddy-covariance sites during the 2003 (panels a, b, e, f, i, j, m, n, o, p) and 2006 (panels c, d, g, h, k, l) European drought events, compared to the Control model (purple line), and to the observations (black line). Grey lines show the prescribed phenologies (LAI, m^2 m^{-2}) and blue bars the daily precipitation (PPT, mm d^{-1}). The Gross Primary Productivity (GPP) is in g C m^{-2} d^{-1} and the Evapotranspiration (ET) in mm d^{-1}.

Fig. 5. A 14-day running average of the carbon and water fluxes predicted by the best selected calibration configuration from the Profit$_{max}$ model (green line) at the five southernmost eddy-covariance sites during the 2003 (panels a, b, e, f, i, j, m, n, o, p) and 2006 (panels c, d, g, h, k, l) European drought events, compared to the Control model (purple line), and to the observations (black line). Grey lines show the prescribed phenologies (LAI, m^2 m^{-2}) and blue bars the daily precipitation (PPT, mm d^{-1}). The Gross Primary Productivity (GPP) is in g C m^{-2} d^{-1} and the Evapotranspiration (ET) in mm d^{-1}.

Fig. 6. A 14-day running average of the carbon and water fluxes predicted by the best selected climate configuration from the Profit$_{max}$ model (green) at the five northernmost eddy-covariance sites during the 2003 (panels a, b, e, f, i, j, m, n, o, p) and 2006 (panels c, d, g, h, k, l) European drought events, compared to the Control model (purple line), and to the observations (black line). The green line is the $k_{max,opt}$ strategy and the green shadings encompass the instantaneous range of fluxes predicted by the three behavioural solutions for k_{max}. Grey lines show the prescribed phenologies (LAI, m^2 m^{-2}) and blue bars the daily precipitation (PPT, mm d^{-1}). The Gross Primary Productivity (GPP) is in g C m^{-2} d^{-1} and the Evapotranspiration (ET) in mm d^{-1}.

Fig. 7. A 14-day running average of the carbon and water fluxes predicted by the best selected climate configuration from the Profit$_{max}$ model (green) at the five southernmost eddy-covariance sites during

the 2003 (panels a, b, e, f, i, j, m, n, o, p) and 2006 (panels c, d, g, h, k, l) European drought events, compared to the Control model (purple line), and to the observations (black line). The green line is the $k_{max,opt}$ strategy and the green shadings encompass the instantaneous range of fluxes predicted by the three behavioural solutions for k_{max}. Grey lines show the prescribed phenologies (LAI, $m^2\ m^{-2}$) and blue bars the daily precipitation (PPT, mm d^{-1}). The Gross Primary Productivity (GPP) is in g C $m^{-2}\ d^{-1}$ and the Evapotranspiration (ET) in mm d^{-1}.

Fig. 8. A comparison of the sensitivity of the Control and calibrated $Profit_{max}$ models' stomatal conductance (g_s) to vapour pressure deficit (D) across the 10 eddy-covariance sites. Panel **(a)** shows the relationship between the implied water use efficiency (g_1, $kPa^{0.5}$) of the calibrated $Profit_{max}$ model and its sensitivity to D (σ, unitless). The values of g_1 obtained for the $Profit_{max}$ model were converted from unit kPa^{σ} to unit $kPa^{0.5}$ for comparison with the values of g_1 used in the Control model. g_1 and σ were obtained by least-square fitting of the g_s simulated by the calibrated $Profit_{max}$ model to the Medlyn *et al.* (2011) stomatal conductance model. The estimates were produced using the site hydraulic and photosynthetic parameters, for temperatures ranging 10 – 40 °C and D ranging 0.05 – 3 kPa. The values of g_1 used in the Control model are plotted against the respective sites' σ for visual comparison with those of the $Profit_{max}$ model only, as they correspond to $\sigma = 0.5$. Panel **(b)** shows the effect of the various σ on the g_s given by the Control model at 25 °C. The input parameter g_1 was set to 2 $kPa^{0.5}$ for all the generated curves, but it was transformed to kPa^{σ} upon running the Control model with the site-specific values of σ shown in panel a. The reference g_s of the Control model ($\sigma = 0.5$) is plotted for comparison. For both panels a and b, the models were run assuming well-watered conditions.

Fig. 9. A comparison of the decline in stomatal conductance (g_s) with predawn soil water potential (Ψ_s), for the Control (plain lines) and the calibrated $Profit_{max}$ (dotted lines) models at a sub-selection of sites. The functional forms emerge from the soil parameters and the β functions in the Control, and from the plant hydraulic traits and the profit maximisation algorithm in the best selected calibration. The inset zooms on the functional forms of the g_s - Ψ_s curves from the Control model for Ψ_s > -0.3 MPa. The functional forms are made comparable by normalising g_s by its maximum at a given site.

Note that seemingly slow decreases in g_s with Ψ_s can be attributed to the non-linear relationship between Ψ_s and volumetric soil moisture, whereby small variations in the latter can lead to large variations in the former. To avoid rainfall effects, the data up to 48 hours after rain were excluded. To avoid low solar radiation and low temperature effects, the g_s data were restricted between 9:00 h – 15:00 h from April – November across all years. The curves were fitted with a linear generalised additive model and the shadings show the 95% confidence interval of the fit.

Fig. 10. The estimated site maximum hydraulic conductance (k_{max}), for each climate configuration of the $\text{Profit}_{\text{max}}$ model and for the best selected calibration, shown as a function of Mean Annual Precipitation (MAP; as listed in Table 2). Note, the MAP was not used in the estimation of k_{max}, however k_{max} was multiplied by the sites' weighted composite LAI, which normalises it to ground area and makes it comparable across sites. Linear regressions are used to show the positive relationship between k_{max} and MAP, with a r^2 of 0.53 and a *p-value* of 0.02 for the best selected calibration, a r^2 of 0.21 and a *p-value* of 0.01 for the Average climate scenario, and a r^2 of 0.30 and a *p-value* of 0.002 for the Extreme climate scenario.

Supporting Information

Additional Supporting Information is available for this article.

Fig. S1 A schematic showing the modelling experiments.

Fig. S2 A 14-day running average of the carbon and water fluxes predicted by the Control model at the five northernmost eddy-covariance sites during the 2003 and 2006 European drought events, compared to the CABLE LSM and to the observations.

Fig. S3 A 14-day running average of the carbon and water fluxes predicted by the Control model at the five southernmost eddy-covariance sites during the 2003 and 2006 European drought events, compared to the CABLE LSM and to the observations.

Fig. S4 The predawn volumetric soil water available to the vegetation, as simulated by the Control model and by CABLE, at the five northernmost eddy-covariance sites during the 2003 European drought event.

Fig. S5 The predawn volumetric soil water available to the vegetation, as simulated by the Control model and by CABLE, at the five southernmost eddy-covariance sites during the 2003 European drought event.

Fig. S6 A 14-day running average of the carbon and water fluxes predicted by two different calibrations of the Control model at a sub-selection of sites in 2002, 2003, 2005, and 2006, compared to the calibrated $Profit_{max}$ model, to the reference Control model, and to the observations.

Fig. S7 A 14-day running average of the carbon and water fluxes predicted by the best selected Calibration at the five northernmost eddy-covariance sites in 2002 and 2005, compared to the Control model and to the observations.

Fig. S8 A 14-day running average of the carbon and water fluxes predicted by the best selected Calibration at the five southernmost eddy-covariance sites in 2002 and 2005, compared to the Control model and to the observations.

Fig. S9 The stomatal conductance as a function of the predawn total volumetric soil water available to the vegetation.

Table S1 Soil parameters at the 10 eddy-covariance sites

Table S2 Plant trait inputs at the 10 eddy-covariance sites

Table S3 Surface properties per plant functional type (PFT)

Table S4 Water available in the five soil-sub layers located below the soil top layer

Table S5 Parameters used in the biochemical photosynthesis model

Table S6 Predicted ranges of k_{max} at the 10 sites compared to species-specific measured values of k_{max}

Methods S1 Biochemical photosynthesis model

Methods S2 Energy balance model

Methods S3 Shape of the vulnerability curves

Methods S4 Coupling carbon and water

Methods S5 Scaling from leaf to canopy

Methods S6 Soil hydrology

Methods S7 Prescribed LAI

Methods S8 Parameter calibrations

Notes S1 Comparison of the Control to CABLE

Notes S2 Why did we not calibrate the Control model?

Notes S3 Comparison of the predicted values of k_{max} to the literature

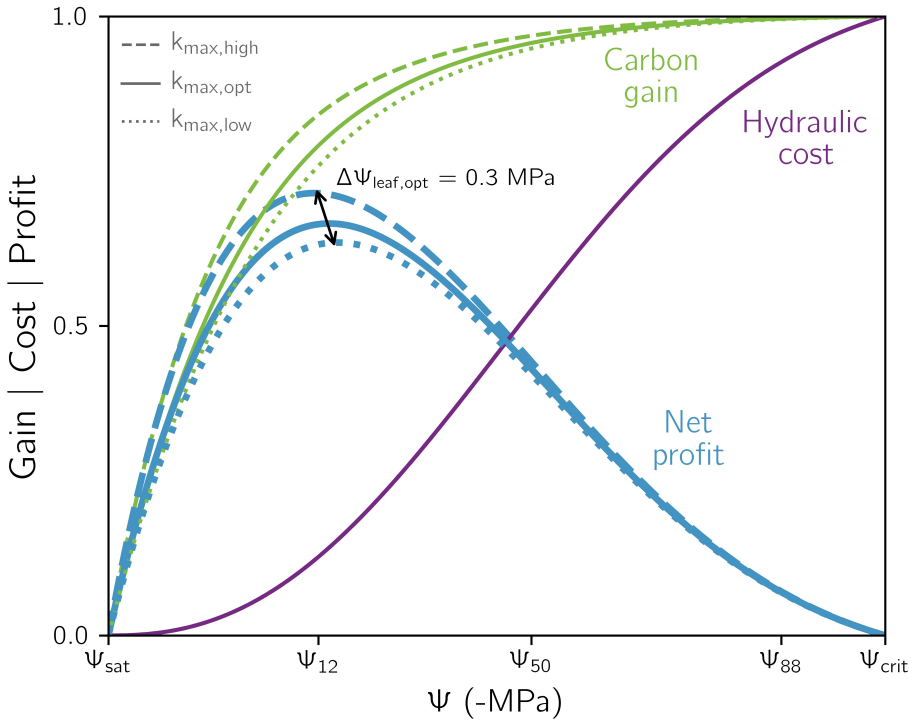

nph_16376_f1.jpeg

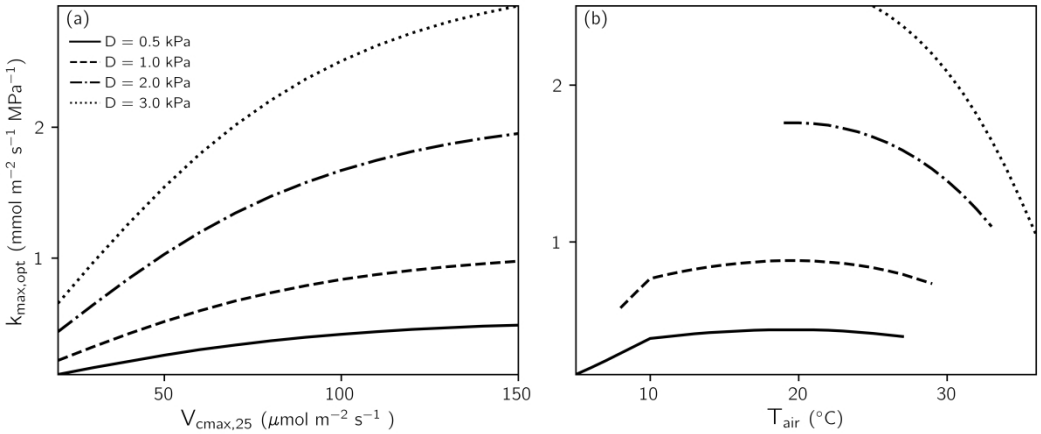

nph_16376_f2.jpeg

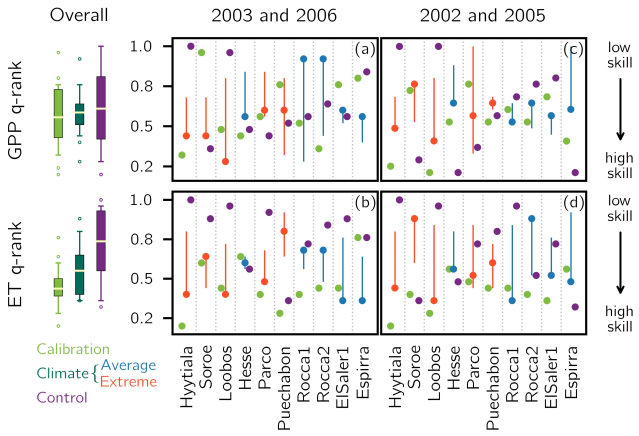

nph_16376_f3.jpeg

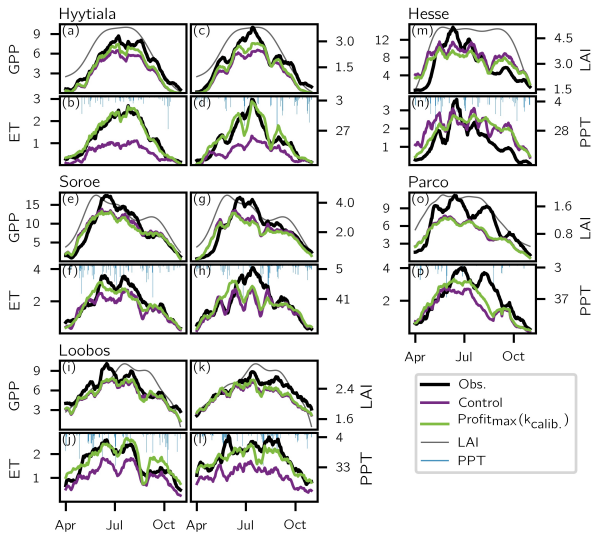

nph_16376_f4.jpeg

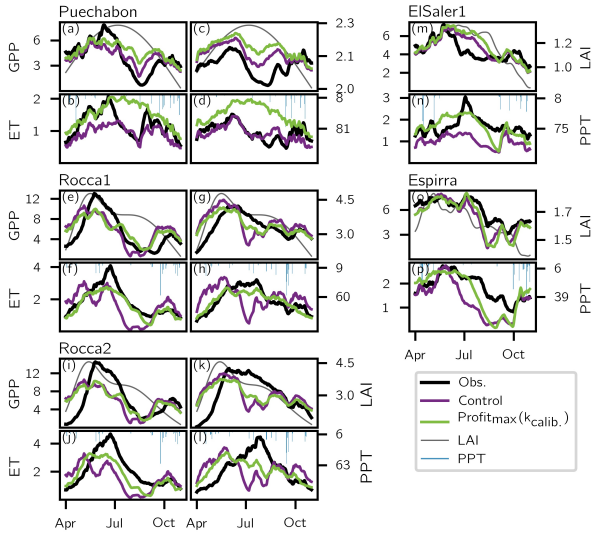

nph_16376_f5.jpeg

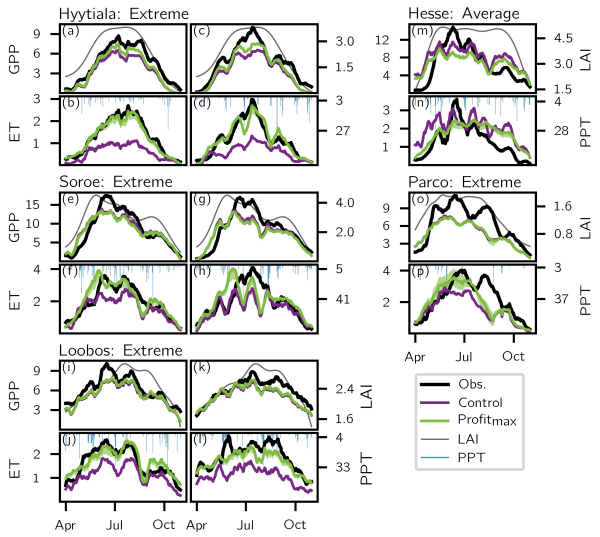

nph_16376_f6.jpeg

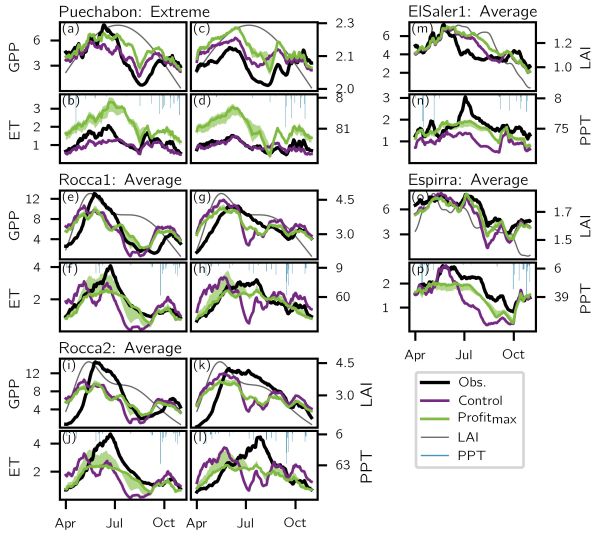

nph_16376_f7.jpeg

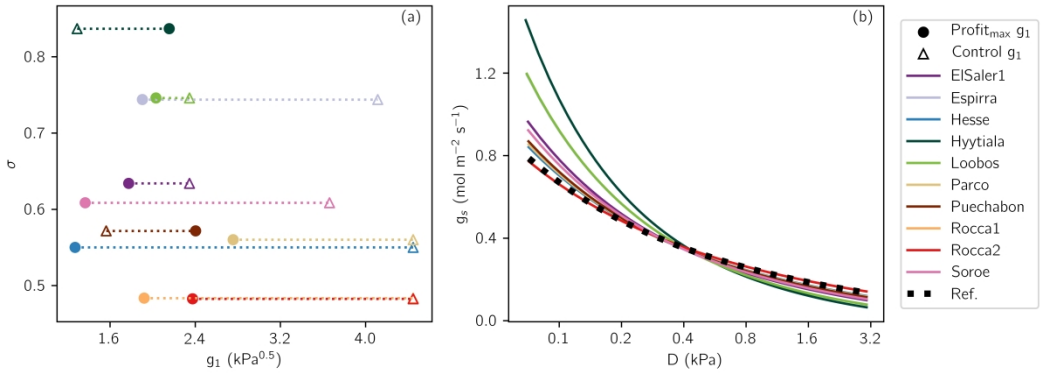

nph_16376_f8.jpeg

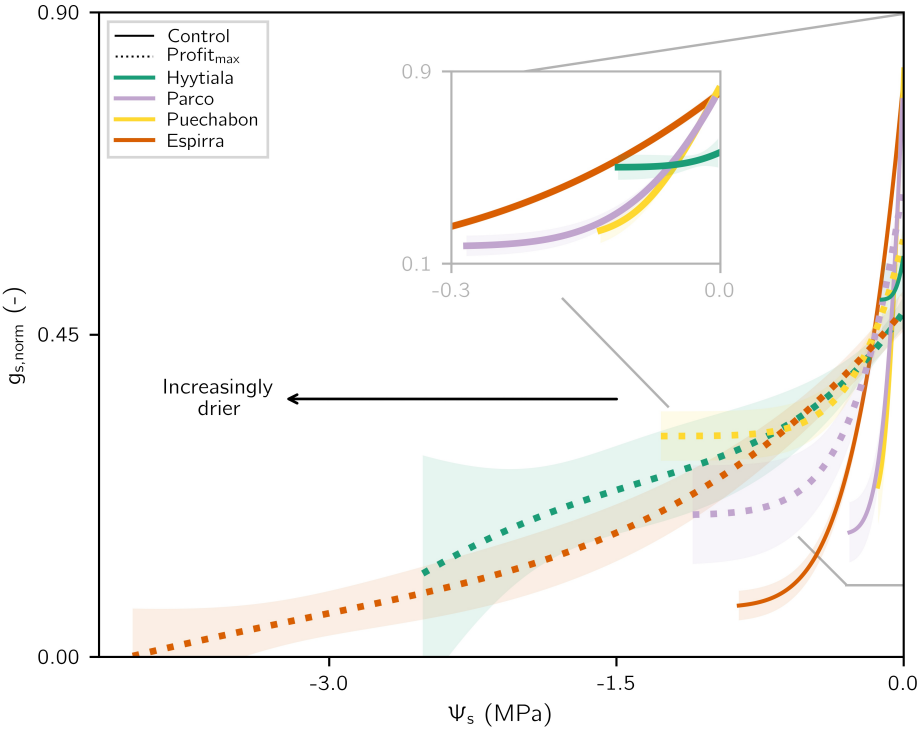

nph_16376_f9.jpeg

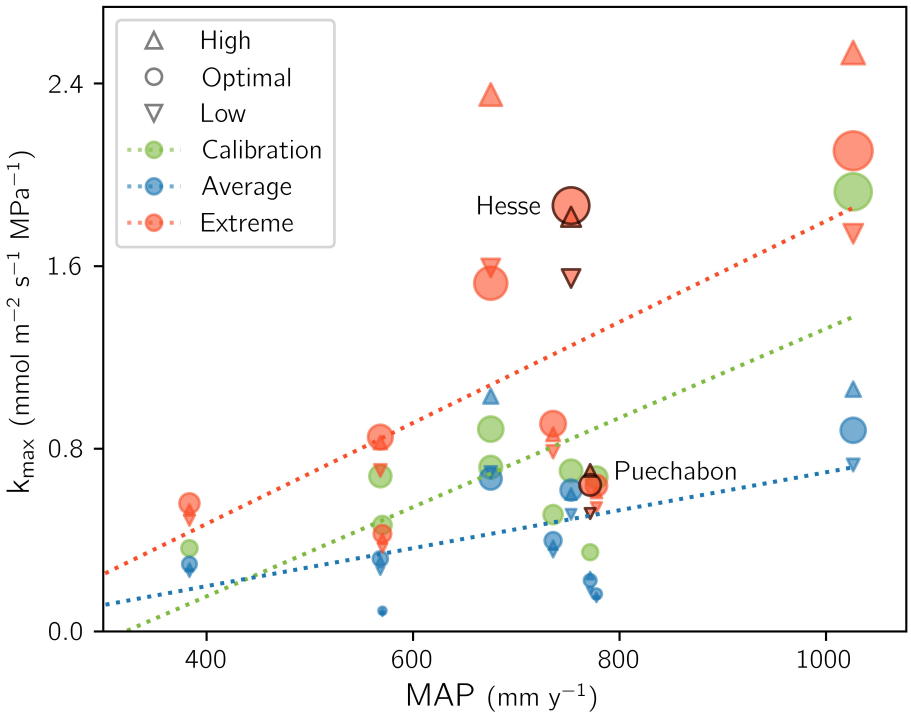

nph_16376_f10.jpeg